Frontiers in Intelligent Colonoscopy

Ge-Peng Ji, Jingyi Liu, Peng Xu, Nick Barnes, Fahad Shahbaz Khan, Salman Khan, Deng-Ping Fan

Abstract—Colonoscopy is currently one of the most sensitive screening methods for colorectal cancer. This study investigates the frontiers of intelligent colonoscopy techniques and their prospective implications for multimodal medical applications. With this goal, we begin by assessing the current data-centric and model-centric landscapes through four tasks for colonoscopic scene perception, including classification, detection, segmentation, and vision-language understanding. This assessment enables us to identify domain-specific challenges and reveals that multimodal research in colonoscopy remains open for further exploration. To embrace the coming multimodal era, we establish three foundational initiatives: a large-scale multimodal instruction tuning dataset ColonINST, a colonoscopy-designed multimodal language model ColonGPT, and a multimodal benchmark. To facilitate ongoing monitoring of this rapidly evolving field, we provide a public website for the latest updates: https://github.com/ai4colonoscopy/IntelliScope.

Index Terms—Colonoscopy, Survey, Vision-language, Multimodal Language Model, Medical Image, Abdomen, Healthcare AI.

✦

1 INTRODUCTION

D ESPITE declining colorectal cancer (CRC) rates in high-income countries, it remains the third most diagnosed cancer worldwide and is increasing in developing countries [1]. Colonoscopy, as an efficient method for CRC screening, utilises a flexible camera-equipped tube to visually examine the colon's interior. As illustrated in Fig. (1-a), this clinical procedure also facilitates intervention with specialised instruments such as snares, forceps, and cautery devices to remove precancerous growths, such as serrated and adenomatous polyps. A recent study [2] indicates that incorporating artificial intelligence (AI) into colonoscopy reduces the miss rate of colorectal neoplasia by approximately 50% compared to traditional methods. This success motivates us to investigate the *frontiers in intelligent colonoscopy*.

Colonoscopy, an endoscopic optical imaging technique, usually presents visual patterns (*e.g.*, non-uniform illumination, homogeneity) that differ from those of general-purpose imaging data, *e.g.*, ImageNet [3], due to the complex and folded anatomy of the colon. This suggests that special methods are needed to interpret the colonoscopic data. In response, we begin with an investigation of the latest intelligent techniques for colonoscopy, assessing the current landscape to sort out domain-unique challenges and underexplored areas. Our analysis reveals that multimodal research in colonoscopy remains largely untapped. To bridge this gap, we contribute three efforts to the community, as illustrated in Fig. (1-b).

Contribution. *(a)* We investigate the latest research progress in four colonoscopic scene perception tasks (refer to Fig. 2)

- Corresponding author: Deng-Ping Fan (dengpfan@gmail.com).
- Deng-Ping Fan is with the Nankai Institute of Advanced Research (SHENZHEN-FUTIAN), Guangdong, China, and also with the College of Computer Science & VCIP, Nankai University, Tianjin, China.
- Ge-Peng Ji and Nick Barnes are with the School of Computing, Australian National University, Canberra, Australia.
- Jingyi Liu is with the Graduate School of Science and Technology, Keio University, Yokohama, Japan.
- Peng Xu is with the Department of Electronic Engineering, Tsinghua University, Beijing, China.
- Fahad Shahbaz Khan and Salman Khan are with Mohamed bin Zayed University of Artificial Intelligence, Abu Dhabi, UAE.

(a) Illustration of a colonoscope inside large intestine (colon)

(b) Highlights of this study

Literature investigation (ColonSurvey)
✓ Four colonoscopy tasks
✓ 63 colonoscopy datasets
✓ 137 related models
✓ Domain challenges

Instruction tuning dataset (ColonINST)
✓ 62 child categories
✓ 300K+ medical images
✓ 128K+ medical captions
✓ 450K+ conversation pairs

Multimodal language model (ColonGPT)
✓ Visual dialogue
✓ Token-efficient design
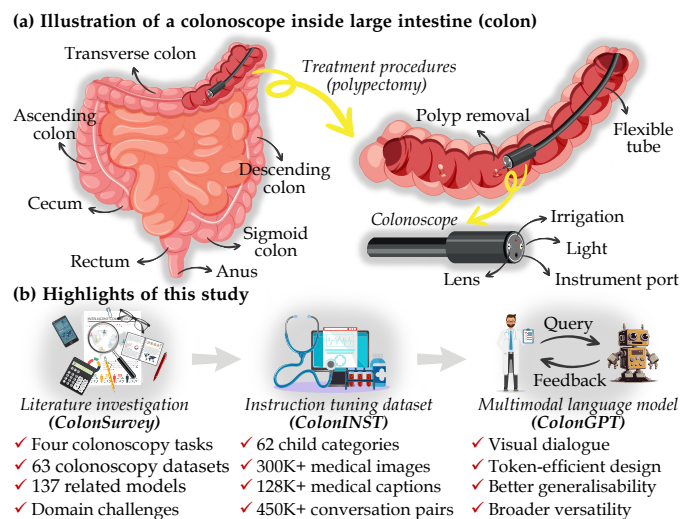✓ Better generalisability
✓ Broader versatility

Fig. 1. **Introductory diagram.** We depict (a) the anatomy of the large intestine (colon) within the digestive tract, the polypectomy procedure during colonoscopy examination, and the components of a colonoscope. The bottom figure (b) summarises three highlights of this study.

from both data-centric and model-centric perspectives. Our investigation summarises key features of 63 datasets and 137 representative deep techniques published since 2015. Additionally, we highlight emerging trends and opportunities for future study. *(b)* We introduce ColonINST, a pioneering instruction tuning dataset tailored for multimodal research, aimed at instructing models to execute user-driven tasks interactively. Assembled from 19 publicly available sources, the ColonINST dataset contains 303,001 colonoscopy images across 62 sub-categories, reflecting diverse scenarios encountered in colonoscopy procedures. We expand these visual samples in two aspects. First, we leverage the multimodal AI chatbot, GPT-4V [4], to generate 128,620 medical captions. Second, we restructure 450,724 human-machine conversations for multimodal adaptation. *(c)* Leveraging the instruction tuning data, we build a multimodal language model, ColonGPT to assist endoscopists through interactive
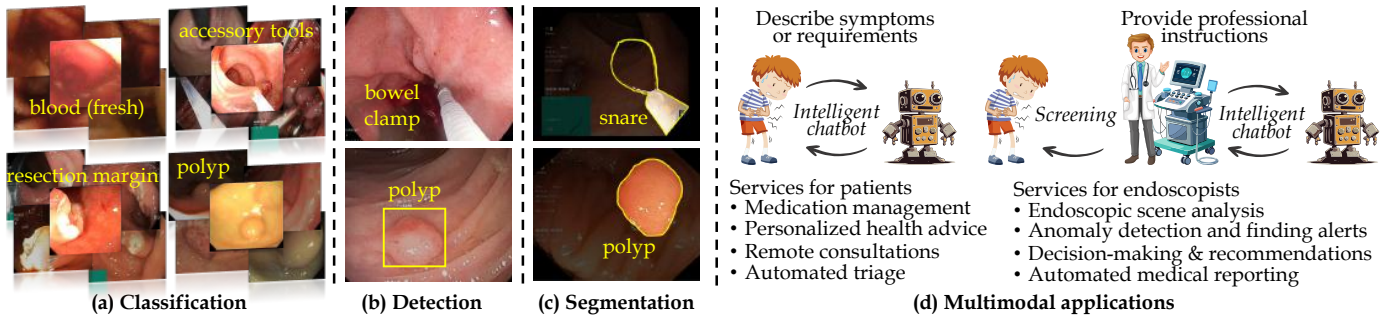
Fig. 2. Colonscopic scene perception from visual to multimodal perspectives. In clinical practice, purely visual tasks, including (a) classification, (b) detection, and (c) segmentation, are applied to identify targets of interest such as polyps and instruments. (d) Multimodal applications improve colonoscopy procedures by performing interactive, user-driven tasks aligned with clinical needs. The chatbot provides personalised advice, automated reporting, and streamline procedural workflows.

dialogues. To ensure reproducibility for average community users, we implement ColonGPT in a resource-friendly way, using a 0.4B-parameter visual encoder SigLIP-SO [5] and a 1.3B-parameter lightweight language model Phi1.5 [6]. Unlike previous vision-language (VL) linking methods [7]–[9] that employ multilayer perceptrons to handle equally all tokens from the visual encoder, we propose a multigranularity adapter to selectively sample visual tokens according to their significance. This strategy reduces the visual tokens to ∼34% of the original number without compromising performance, securing the top spot in our newly-created multimodal benchmark across three tasks. Importantly, our ColonGPT can be trained within five hours on four A100-40GB GPUs, facilitating rapid proof-of-concept development for subsequent research.

Scope. This study differs from previous works in several aspects. Earlier surveys on traditional [10] and deep learning [11]–[14] methods conducted before 2020 are now out of date. Although a recent study [15] explores various applications of colonoscopy, such as quality analysis and abnormality detection, it lacks numerical validation. Other benchmarks [16]–[18] are limited to specific narrow research subfields. By contrast, we delve into four tasks for colonoscopic scene perception and evaluate their current state to sort out key challenges and under-researched areas. Importantly, our vision goes beyond by laying the foundations for the coming era, a multimodal world. To embrace this era, we further undertake three initiatives: a multimodal instruction tuning dataset, a multimodal language model, and a multimodal benchmark for the community.

Organisation. The remaining sections are structured as such: §2 provides a historical background and discusses the domain-unique challenges. §3 investigates 63 colonoscopy related datasets, followed by a survey of 137 deep models in §4. In §5, we introduce three initiatives towards the multimodal era: the creation of ColonINST, the technical details of ColonGPT, and a comparative multimodal benchmark along with ablative analyses. Finally, this paper is concluded in §6.

2 BACKGROUND

2.1 Origin and evolution

The history of colonoscopy has two key milestones. In 1968, gastrointestinal surgeons Hiromi Shinya and William Wolff

found a link between colonic polyps and intestinal tumours, but they lacked equipment to examine them. In 1969, they discovered Corning Incorporated's optical fibres and collaborated with Olympus to create the fiberoptic colonoscope, a groundbreaking device to examine the colon and remove polyps using wire loops. The second milestone came in 1983 with the introduction of the electronic colonoscope [79], which allows visualisation of the colon on a screen and polyp removal using a polypectomy snare, enhancing detection rates and reducing bleeding. The 21st century brings the AI era, where computer-aided diagnosis systems provide greater precision and reliability in procedures [80]. This study explores the transformative impact of intelligent techniques for colonoscopy, which is a type of endoscopy [81], while other related techniques such as laparoscopy [82] are summarised in our appendix.

2.2 Intrinsic traits and domain-unique challenges

We summarise five unique challenges associated with colonoscopic vision tasks, primarily caused by procedural aspects and imaging conditions during a colonoscopy. *(a) Non-linear camera ego-motion.* Procedural constraints force the camera (*i.e.*, colonoscope) to actively move in a non-linear and unpredictable manner, challenging ego-motion compensation [83] and causing motion blur [62]. *(b) Presence of medical instruments.* The colonoscopy procedure often includes instruments such as scopes, guidewires, and snares, which should be distinguished properly from anatomical structures [84] for efficient analysis. *(c) Limited observable field.* The intricate folds and blind spots within the colon restrict the visible area in colonoscopy data. This requires algorithms capable of extracting relevant information from limited visual landscapes [85]. *(d) Non-uniform illumination.* The mucosal surface of the colon, prone to wetness and sheen, results in highly variable and diffuse illumination with complex reflections such as non-Lambertian reflections and interreflections. Traditional lighting-based algorithms struggle under these conditions [86]. *(e) Variability in tissue appearance.* Mucosal textures and colours vary considerably due to constant movement, disease states, anatomical differences, and instrument effects. Furthermore, benign polyps or lesions usually have weak or homogeneous boundaries [87], making them blend into surrounding tissues and difficult to detect. These issues require a robust response from AI models to inherent morphological and colour fluctuations.

TABLE 1

Data statistics for colonoscopy datasets. The columns include: number of images (#IMG) and videos (#VID), classification tag (Cls), bounding box (Bbx), segmentation mask (Seg), text (Tx). The categories not related to colonoscopy, such as stomach and esophagitis, are marked in grey.

Dataset	Publication	#IMG	#VID	Cls	Bbx	Seg	Tx	Number of categories (#C) → Category names	URL
CVC-ColonDB [19]	PR'12	300	15			✓		#C1 → polyp	Link
ETIS-Larib [20]	CARS'14	196	-			✓		#C2 → polyp, non-polyp	Link
CVC-ClinicDB [21]	CMIG'15	612	31			✓		#C1 → polyp	Link
ASU-Mayo [22]	TMI'15	36,458	38	✓				#C2 → polyp, non-polyp	Link
Ye et al. [23]	MedIA'16	7,894	10	✓	✓			#C2 → polyp, non-instance	Link
Deeba et al. [24]	IJCNN'16	100	-	✓				#C2 → bleeding, non-bleeding	-
CU-ColonDB [25]	JBHI'16	1,930	-	✓				#C3 → hyperplasia polyps, adenomatous polyps, non-polyp	-
ColonoscopicDS [26]	TMI'16	-	76	✓				#C3 → serrated adenomas, hyperplastic lesions, adenoma	Link
CVC-ClinicVideoDB [27]	MICCAIw'17	10,924	18	✓	✓	✓		#C2 → polyp, non-polyp	Link
Kvasir [28]	MMSys'17	8,000	-	✓				#C8 → cecum, polyps, ulcerative colitis, dyed and lifted polyp, dyed resection margins, Z-line, pylorus, esophagitis	Link
Nerthus [29]	MMSys'17	5,525	21	✓				#C4 → BBPS (Boston-Bowel-Preparation-Scale) 0/1/2/3	Link
EndoSceneStill [30]	JHE'17	912	44			✓		#C1 → polyp	Link
KID1 [31]	EIO'17	137	-	✓				#C10 → angiectasias, ulcers, stenoses, villous edema, nodular lymphangiectasias, chylous cysts, polyps, aphthae, normal/no pathology, intraluminal hemorrhage	Link
KID2 [31]	EIO'17	2,371	47	✓		✓		#C4 → vascular anomalies, polypoid anomalies, inflammatory anomalies, normal images	Link
NBIPolyp-UCdb [32]	BSPC'19	86	11			✓		#C2 → adenomas, hyperplastic	Link
WLPolyp-UCdb [33]	EIO'19	3,040	42	✓				#C2 → polyp, normal mucosa	Link
ASEI [34]	MM'19	4,470	-	✓	✓			#C4 → dyed-lifted-polyps, dyed-resection-margins, instruments, polyp	Link
Cho et al. [35]	PeerJ'19	328,927	112	✓				#C1 → cecum	Link
EAD2019 [36]	arXiv'19	2,342	-		✓	✓		#C7 → imaging artefacts, contrast, specularity, instrument, bubbles, motion blur, saturation	Link
Liu et al. [37]	ISBI'20	14,317	18	✓				#C2 → polyp, non-polyp	-
Kvasir-SEG [38]	MMM'20	1,000	-		✓	✓		#C1 → polyp	Link
PICCOLO [39]	ApplSci'20	3,433	39	✓		✓		#C17 → Paris classification (protruded lesions: 0-Ip/0-Ips/0-Is, elevated lesions: 0-IIa/0-IIa+c, flat lesions: 0-IIb), NICE classification (type 1/2/3), Diagnosis (adenocarcinoma/adenoma/hyperplasia), Histological stratification (high grade dysplasia/hyperplasia/invasive adenocarcinoma/low grade dysplasia/no dysplasia)	Link
EDD2020 [40]	arXiv'20	386	-		✓	✓		#C5 → suspicious area, high-grade dysplasia, adenocarcinoma, polyp, normal dysplastic Barrett's oesophagus	Link
CAD-CAP [41]	EIO'20	25,124	1,686	✓		✓		#C4 → vascular lesions, fresh blood, ulcero-inflammatory lesions, normal images	-
ACP-ColonDB$_{530}$ [42]	NPJDM'20	221,976	-		✓	✓		#C13 → adenomatous polyp, hyperplastic polyp, other polyp, bleeding, IC valve, instrument, artefact, normal colon structure, bubble, inside colon background, stool, lumen, outside colon background	-
HyperKvasir [43]	SData'20	110,079	374	✓		✓	✓	#C23 → cecum, retroflex rectum, BBPS 0-1/2-3, ulcerative colitis grade 1/2/3/0-1/1-2/2-3, polyps, dyed lifted polyps, dyed resection margins, hemorrhoids, Barrett's, terminal ileum, Z-line, esophagitis grade A, esophagitis grade B-D, pylorus, retroflex stomach, Barrett's (short-segment), impacted stool	Link
WCE-Polyp [44]	TMI'20	541	-			✓		#C1 → polyp	Link
EAD2020 [45]	MedIA'21	2,531	-			✓		#C8 → specularity, bubbles, saturation, contrast, blood, instrument, blur, imaging artefacts	Link
BKAI-Small [46]	ISVC'21	1,200	-			✓		#C3 → non-neoplastic polyp, neoplastic polyp, background	Link
BKAI-Large [46]	ISVC'21	7,466	-			✓		#C4 → non-neoplastic polyp, neoplastic polyp, undefined polyp, background	Link
CPC-Paired [47]	MICCAI'21	681	-	✓	✓			#C2 → hyperplastic polyp, adenoma	Link
LDPolyVideo [48]	MICCAI'21	901,666	263	✓	✓			#C2 → polyp, non-polyp	Link
Celik et al. [49]	MICCAI'21	2,224	-		✓			#C2 → polyps, Barrett's esophagus	Link
Kvasir-Instrument [50]	MMM'21	590	-		✓	✓		#C1 → GI procedure tools (e.g., snares, balloons, and biopsy forceps)	Link
CP-CHILD [51]	BMCMI'21	9,500	-	✓				#C2 → colonic polyp, normal or other pathological images	Link
CROHN-IPI [52]	EIO'21	3,498	-	✓				#C7 → erythema, edema, aphthoid ulceration, ulceration (3–10mm, >10mm), stenosis, non-pathological	Link
C-E Crohn's Disease [53]	FMOLB'21	467	164	✓		✓		#C1 → Crohn's lesions	-
SUN-database [54]	GIE'21	159,232	113	✓	✓			#C7 → hyperplastic polyp, low grade adenoma, high-grade adenoma, traditional serrated adenoma, invasive carcinoma, sessile serrated lesion, negative	Link
Kvasir-Sessile [55]	JBHI'21	196	-			✓		#C1 → polyp (<10mm)	Link
Kvasir-Capsule [56]	SData'21	4,741,504	117	✓	✓			#C14 → polyp, Ileocecal valve, lymphangiectasia, erythema, angiectasia, foreign body, erosion, ulcer, blood (fresh), blood (hematin), normal clean mucosa, reduced mucosal view, pylorus, ampulla of Vater	Link
KUMC [57]	PONE'21	37,899	155	✓	✓			#C2 → hyperplastic polyps, adenomatous polyps	Link
ERS* [58]	arXiv'22	1,354,667	1,520	✓			✓	#C27 → ulcerative colitis (active/quiescent), stricture (postoperative/inflammatory/malignant), polyp, melanosis, diverticulosis, fistula, crohnsdisease (active/quiescent), lipoma, proctitis, hemorrhoids, submucosal tumor, solitary ulcer, bleeding of unknown origin, ileitis, diverticulitis, colitis: ischemic, colorectal cancer, angiodysplasia, rectal ulcer, foreign body, polyposis syndrome, postoperative appearance, parasites	Link
Tian et al. [59]	MICCAI'22	807,069	253	✓	✓			#C2 → polyp, non-polyp	Link
WCE-CCDD [60]	BSPC'22	6,000	-	✓				#C4 → ulcer, polyps, normal, esophagitis	Link
PolypGen2.0 [61]	ISBIw'22	3,446	46	✓	✓	✓		#C2 → serrated, adenomas	Link
SUN-SEG [62]	MIR'22	159,232	1,013	✓	✓	✓		#C7 → hyperplastic polyp, low grade adenoma, high-grade adenoma, traditional serrated adenoma, invasive carcinoma, sessile serrated lesion, negative	Link
SinGAN-Seg [63]	PONE'22	10,000	-			✓		#C1 → polyp	Link
ENDOTEST [64]	SJG'22	253,754	58	✓	✓			#C2 → polyp, non-polyp	Link
MEDVQA-GI [65]	CLEF'23	3,949	-				✓	#C2 → polyp, surgical equipment	Link
GastroVision [66]	ICMLw'23	8,000	-	✓				#C27 → accessory tools, angiectasia, blood in lumen, cecum, colon diverticula, resection margins, colorectal cancer, dyed-lifted-polyps, erythema, ulcer, dyed-resection-margins, retroflex rectum, mucosal inflammation large bowel, resected polyps, colon polyps, Ileocecal valve, normal mucosa and vascular pattern in the large bowel, esophagitis, Barrett's esophagus, duodenal bulb, esophageal varices, gastric polyps, gastroesophageal junction normal z-line, normal esophagus, normal stomach, pylorus, small bowel terminal ileum	Link
W-Polyp [67]	CVPR'23	1,450	-			✓		#C1 → polyp	Link
LIMUC [68]	IBD'23	11,276	-	✓				#C4 → Mayo endoscopic score (MES) 0/1/2/3	Link
PS-NBI2K [16]	JBHI'23	2,000	-			✓		#C1 → polyp	Link
PolypGen [69]	SData'23	8,037	23	✓	✓	✓		#C2 → polyp, negative	Link
MedFMC** [70]	SData'23	22,349	-	✓				#C5 → ulcer, erosion, polyp, tumor, and non-instance	Link
GB-WCE Dataset [71]	MD'23	226	-	✓				#C2 → bleeding or lesions, normal	Link
REAL-Colon [72]	SData'24	2,757,723	60		✓			#C2 → polyp, negative	Link
Xu et al. [73]	TMI'24	251	-	✓				#C4 → Mayo endoscopic score (MES) 0/1/2/3	Link
Kvasir-VQA [74]	MMw'24	6,500	-	✓			✓	#C5 → polyps, ulcerative colitis, instrument, normal, esophagitis	Link
CapsuleVision2024 [75]	CVIP'24	58,124	-	✓				#C10 → angioectasia, bleeding, erosion, erythema, foreign body, lymphangiectasia, polyp, ulcer, worms, normal	Link
COLON [76]	arXiv'24	~430,000	30	✓	✓	✓		#C3 → adenoma, hyperplastic, non-pathological case	Link
WCEBleedGen [77]	arXiv'24	2,618	-		✓	✓		#C2 → bleeding, non-bleeding	Link
PolypDB [78]	arXiv'24	3,934	-		✓	✓		#C1 → polyp (multiple imaging modalities and multiple medical centers)	Link

*NOTE – The ERS dataset [58] includes 99 annotated categories in total. For the sake of brevity, we list only 27 colon-related categories within ERS.
**NOTE – The MedFMC dataset [70] comprises 23,349 medical images across five modalities. This table only enumerates the categories specific to the endoscopic modality.

3 REVISITING COLONOSCOPY DATA

3.1 Medical data for colonoscopy

Tab. 1 presents our investigation of 63 datasets with their essential statistics for four tasks related to colonoscopic scene perception. We search for them using queries such as "colonoscopy dataset/benchmark" and "gastrointestinal disease dataset". They consist of images or videos related to the human colon. In particular, some datasets also include images of other organs, such as the pylorus in [28] or the stomach in [66]. Next, we review these selected datasets according to their different task objectives.

• **Classification datasets** have been widely used for varied purposes, such as colon disease classification in images [28], [31], [40], [43], [52], [58], [60], [66], [68], [73], [75]/videos [54], [56], [62], polyp identification [27], [33], [37], [39], [41], [48], [51], fine-grained polyp classification [25], [26], [47], bleeding condition [24], [71], [77], anomaly recognition [59],

cecum recognition [35], and pre-operative assessment [29].

• **Detection datasets** provide both categorical and localisation labels for targets of interest, such as colonic diseases [54], [57], [62], accessory instruments [34], [42], [42], polyps [23], [48], [59], [64], [72], endoscopic artefacts [36], [45], and gastrointestinal diseases [43], [56]. In addition, the organisation of competitions has accelerated growth within the colonoscopy community by establishing shared platforms for data collection and model evaluation, significantly advancing research areas such as the detection of intestinal disease [40] and polyp [38], [61], [69].

• **Segmentation datasets** for colonoscopy research originate from two sources. The first source comprises real data, mainly utilised for single-target segmentation of entities such as polyps [16], [30], [32], [33], [44], [49], Crohn's disease [53], and accessory tools [50]. Some datasets, like BKAI-Small/Large [46], provide instance-level masks for neoplastic and non-neoplastic polyps. Other datasets come from organised competitions, such as polyp segmentation datasets [19]–[22], [61] and a gastrointestinal diseases segmentation dataset [40], or extensions of existing databases, offering pixel-wise masks (*e.g.*, for polyps [38], [55], colorectal disease [62]) or scribble labels (*e.g.*, for polyps [59], [67]). The other source, such as SinGAN-Seg [63], generates synthetic images for polyp segmentation.

• **VL datasets** remain relatively scarce so far, with two known datasets for this specific purpose. MEDVQA-GI [65] contributes the first dataset with three VL tasks, including visual question answering, visual question generation, and visual location question answering. Kvasir-VQA [74] collects 6,500 question-answer pairs from existing datasets [43], [50], for gastrointestinal diagnostics, such as image captioning, visual question answering.

3.2 Discussion

Based on the 63 revisited datasets, we have several data-centric observations that could inspire more future ideas.

• **Data granularity** requires improvement to better understand patient conditions and treatment efficacy. *(a)* More than a quarter of polyp-containing datasets provide fine-grained categorisation, often with inadequate detail. For example, BKAI-Small/-Large [46] provide two instance annotations of neoplastic and non-neoplastic polyps. ColonoscopicDS [26] categorises at the video level into hyperplasic, serrated, and adenoma lesions. SUN-database [54] provides fine-grained labels, documenting measurements of polyp size (height, width) and morphology (pedunculated, sessile, flat), along with their anatomical locations (*e.g.*, rectum, sigmoid colon). Several data-centric areas remain under-explored, such as temporal lesion evolution recording, granularity improvement, graded severity tagging, and instance-level target annotation. *(b)* Furthermore, label orthogonality, an often overlooked issue, treats labels as isolated entities. Current works seldom discuss potential inter-class correlations, such as the co-occurrence of inflammatory bowel disease with erosion symptoms, Crohn's disease with fistula complications, or colorectal cancer accompanied by bleeding. Future studies should consider causality [88] and comorbidity [89] to address these correlations effectively.

• **Data diversity** is crucial to developing fair and reliable models. Three aspects deserve consideration. *(a)* Datasets for rare colorectal diseases appear to be limited, due to case scarcity and expertise requirements. For example, Crohn's disease, which affects an estimated 58 to 241 per 100,000 adults in the United States [90], has so far been discussed in three datasets [52], [53], [58]. Such an unbalanced situation leads to data-hungry models performing better in common cases than in rarer or novel ones. Thus, increasing attention to rare gastrointestinal diseases could potentially improve the ability to treat long-tailed [91] or open-vocabulary [92] problems. *(b)* Multimodal research in colonoscopy appears to be in its early stages, with limited data [65], [74] for analysis. Therefore, collecting varied patient information (*e.g.*, age, gender, eating habits) combined with expert interpretations (*e.g.*, clinical report, medication advice) could be advantageous and ultimately facilitate personalised and side-effect-minimised colonoscopy practices [93].

• **Data inconsistency** in colonoscopy research is due to two main factors. *(a)* Expert interpretations vary due to varying experience, expertise, and observed nuances, leading to subjective judgements and labelling uncertainties. For example, ColonoscopicDS [26] provides raw diagnostic labels for each sample from multiple experts and beginners, reflecting their underlying (dis)agreement. In addition, SUN-SEG [62] releases the rejected segmentation masks from their annotation workflow, highlighting the challenges in reaching consistent polyp boundaries. *(b)* Existing datasets often have study-specific targets, leaving others unlabelled or classified as background. Nerthus [28], for example, focuses on assessing the quality of bowel preparation, but ignores diagnostic findings such as polyps. Furthermore, multiple categories in GastroVision [66] are not mutually exclusive; for example, a case labelled as "accessory tool" could also fall into the category "blood in lumen". Segmentation data like Kvasir-Instrument [50] annotates only medical instruments, ignoring other targets like polyps, whereas Kvasir-SEG [38] provides polyp label, leaving out others like instruments. These observations prompt future research into learning from partial [94], noisy [95], or missing [96] labels.

4 REVISITING COLONOSCOPY MODELS

In this section, we investigate 137 deep learning models for colonoscopic scene perception, sourced from leading conferences or journals published since 2015. First, three widely recognised topics are described, including 18 classification models (§4.1), 24 detection models (§4.2), and 86 segmentation models (§4.3). Their architectural designs are classified into five subtypes as presented in Fig. 3. Lastly, we discuss nine VL-related models in §4.4.

4.1 Classification models

• **Input phase.** Tab. 2 lists the training and testing data used for each deep model. We note that many classification models [106], [109], [112]–[114], [116], [118] in colonoscopy use in-house data for model development, partly resulting in the absence of domain-recognised benchmarks. This issue stems from the different categorical goals pursued by individual studies, such as identifying polyps from white-light and narrow-band imaging pairs [47], [111], images [106], or videos [59], evaluating polyp size [116], and recognising colonic diseases [112] or landmarks [119].

TABLE 2
Summary of classification models in colonoscopy. <u>Dataset:</u> CU=CU-ColonDB [25], CDS=ColonoscopicDS [26], Private=private data, HK= HyperKvasir [43], KC=Kvasir-Capsule [56]. <u>Backbone:</u> CaffeNet [97], D-121=DenseNet121 [98], R-12/-18/-50/-101=ResNet12/18/50/101 [99], ViT-S16 or ViT-B16 [100], MobV2=MobileNetV2 [101], R50-Att=ResNet50 with attention module [102], C3D [103], Inc-v3=Inception3 [104], I3D [105]. "Customised" means a base network modified for the current task or a model independent of the base network choice. <u>Head:</u> classifier implemented by the fully connected (FC) and support vector machine (SVM) layers, or using the ℓ^2 norm to measure the disparity between the input and output. <u>Arch:</u> the architectures shown in Fig. 3. Sup: learning strategies such as fully supervised (FS), semi-supervised (SS), unsupervised (US), and weakly supervised (WS). For simplicity, the following tables use consistent abbreviations unless specified otherwise.

|	Model	Publication	Core design	Training dataset	Testing dataset	Backbone	Arch	Head	Sup	URL
Image-based models	Zhang *et al.* [25]	JBHI'16	domain transfer learning	CU, CDS	CU, CDS	CaffeNet	BF#1	SVM	FS	-
	RIIS-DenseNet [106]	MICCAI'18	rotation-invariant, similarity constrained	Private	Private	D-121	SF	FC	FS	-
	FSAD-Net [107]	MICCAI'20	mutual information maximisation	Private	Private	D-121	BF#2	FC	US	Link
	Gammulle *et al.* [108]	MICCAI'20	relational mapping	Kvasir [28], Nerthus [29]	Kvasir [28], Nerthus [29]	R-50	MF#1	FC	FS	-
	ADGAN [37]	ISBI'20	dual adversarial learning	Liu *et al.* [37]	Liu *et al.* [37]	Customised	BF#2	ℓ^2	US	-
	Carneiro *et al.* [109]	MedIA'20	model uncertainty & calibration	Private	Private	D-121	SF	FC	FS	-
	SSL-WCE [110]	MedIA'20	adaptive aggregated attention	CAD-CAP [41]	CAD-CAP [41]	D-121	BF#2	FC	SS	Link
	PolypsAlign [47]	MICCAI'21	teacher-student alignment	CPC-Paired [47]	CPC-Paired [47]	R-50	BF#2	FC	FS	Link
	CPC-Trans [111]	MICCAI'22	cross-modal representation consistency	CPC-Paired [47]	CPC-Paired [47]	ViT-S16	BF#2	FC	FS	Link
	FFCNet [112]	MICCAI'22	frequency domain learning	Private	Private	R-18	SF	FC	FS	Link
	DLGNet [113]	MedIA'23	Gaussian mixture model	Private	Private	R-18	BF#2	FC	FS	Link
	Yue *et al.* [114]	TIM'23	class imbalance loss	Private, HK	Private, HK	MobV2	SF	FC	FS	Link
	DAFON [115]	ESWA'24	few-shot open-set learning	Kvasir-Capsule [56]	Kvasir-Capsule [56]	R-12	BF#2	FC	FS	-
	SSL-CPCD [73]	TMI'24	composite pretext-class discrimination	LIMUC [68]	Private, LIMUC [68]	R50-Att	BF#2	FC	FS	Link
Video	BseNet [116]	MICCAI'18	unsupervised depth estimation, LSTM [117]	Private	Private	C3D	SF	FC	FS	-
	Byrne *et al.* [118]	Gut'19	real-time assessment system	Private	Private	Inc-v3	SF	FC	FS	-
	Tamhane *et al.* [119]	MICCAIw'22	vision transformer based	Private	Private	ViT-B16	SF	FC	FS	-
	Tian *et al.* [59]	MICCAI'22	multiple instance learning	WVAD [59]	WVAD [59]	I3D	SF	FC	WS	Link
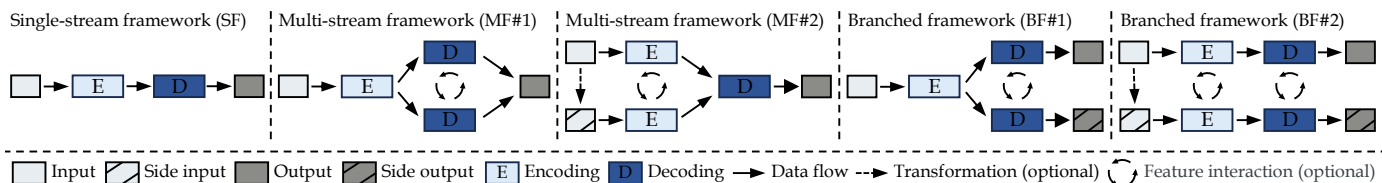
Fig. 3. **Gallery of deep-based architectures.** The single-stream framework (SF) features a single input and output with sequential data flow. Multi-stream frameworks predict a single output but involve parallel processing streams, either at the decoding stage (MF#1) or the encoding stage (MF#2). Branched frameworks extend multi-stream framework to produce multiple outputs from either a single input (BF#1) or multiple inputs (BF#2). These side outputs typically receive supervision from additional supervisory signals, such as boundary cues.

• **Processing phase.** We discuss data flow management strategies based on two attributes. *(a) Backbone:* Early models [106], [108] typically employ well-trained convolutional backbones (*e.g.*, ResNet [99], DenseNet [98]) from ImageNet [3], while recent studies explore alternatives such as using a vision transformer in [111] and a lightweight network in [114]. Another strategy is SSL-CPCD [73], which involves pre-training a model to generate domain-specific representations, followed by its generalisation on various downstream perception tasks. *(b) Architecture:* Classification models involve various designs as in Fig. 3. At first, a basic idea is of using a single-stream framework (SF) that sequentially processes visual features based on confidence calibrated [109] or 3D convolutional [59], [116] networks. Second, Gammulle *et al.* [108] proposed a dual decoding flow approach for hierarchical feature encoding, typified as MF#1. Third, to ensure reliable predictions, branched frameworks are adopted for multi-objective learning, such as the integration of parallel feature flows [25], interclass Gaussian loss [113], and global-to-local consistency [111].

• **Output phase.** *(a) Prediction head:* An early model [25] applies two SVM layers to classify polyps into three categories. Modern methods usually adopt a fully connected layer as the final classifier due to its simplicity and flexibility. A special case is ADGAN [37], a generative adversarial network that computes the ℓ^2 norm differential between input and output to identify anomalous images. *(b) Supervision strategy:* Most methods use fully-supervised learning with pre-annotated categories, but some explore data-efficient strategies, including semi-supervised [110], weakly-supervised [59], and unsupervised [37], [107] learning.

• **Remarks.** We observe three aspects of the above classification models. *(a)* Novel visual backbones, like the state space model [149], remain underexplored. Furthermore, reformulating the classification paradigm within VL models, *e.g.*, CLIP [150], can yield unexpected results. *(b)* Benchmarks for multicategory classification remain underexplored. The Kvasir series [28], [43], [56] offers valuable sources for further study. We will explore these public data on their potential synergy in §5.1. *(c)* Several new task settings have emerged in colonoscopy. For example, Tian *et al.* [59] recognise abnormal frames from colonoscopy videos from an out-of-distribution view. DAFON [115] solve an open-set classification problem within a few-shot framework.

4.2 Detection models

• **Input phase.** Detection models classify targets and locate them using boxes, assisting surgical intervention and planning. The goals of interest are diverse, such as identifying the polyp(s) in images [126]–[128], [130]–[134], [136]/videos [22], [137]–[139], [141]–[148], or locating multiple findings [42] like bleeding, polyps, and accessory tools.
• **Processing phase.** This has three key configurations for the analysis. *(a) Backbone:* There are two general strategies for network initialisation. The first group [42], [126]–[128], [131], [132], [134], [136], [143], [146]–[148] leverages the ResNet series [99] pre-trained on the ImageNet [3] dataset. The second group relies on well-trained object detectors, such as [130], [142] using DarkNet series [120], [121] and [133] employing EfficientDet-D0 [122]. *(b) Workflow:* Detection models are often built on general-purpose architectures. In the "WF" column of Tab. 3, we categorise the models according to

TABLE 3
Summary of detection models in colonoscopy. <u>Dataset</u>: C6=CVC-ClinicDB [21], ETIS=ETIS-Larib [20], ASEI=ASEI [34], C3=CVC-ColonDB [19], KUMC [57], LDPV=LDPolyVideo [48], SUN=SUN-database [54], PL=PICCOLO [39], KID=KID1&2 [31], CDS [26], KSe=Kvasir-Sessile [55], ASU=ASU-Mayo [22], CDB=CVC-ClinicVideoDB [27], ES=EndoSceneStill [30], CU [25], ACP=ACP-ColonDB530 [42]. <u>Backbone</u>: R-34/-50/-101 [99], CDN-53=CSPDarkNet53 [120], DN-53=DarkNet-53 [121], EffDet-D0=EfficientDet-D0 [122], AlexNet [123], V-16=VGG16 [124], R-50v2=ResNet50V2 [125]. <u>WF</u>: one-stage (OS) or two-stage (TS) workflows. <u>NMS</u>: non-maximum suppression. <u>EC</u>: edge-sensitive cues.

	Model	Publication	Core design	Training dataset	Testing dataset	Backbone	WF	Arch	NMS	EC	Sup	URL
Image-based models	Yang et al. [126]	TIM'20	parallel detection & segmentation	Private, C6, ETIS	Private, C6, ETIS	R-50	TS	BF#1			FS	-
	ConsolidatedPolypDA [127]	MedIA'21	Gaussian Fourier domain adaptation	C6	ETIS, ASEI	R-101	TS	BF#2			US	Link
	MDeNetplus [128]	MedIA'21	2D Gaussian shapes prediction	C6	C3, ETIS	R-34	OS	MF#1		✓	FS	-
	FedInI [129]	MICCAI'22	federated learning, structural causal model	KUMC	KUMC	R-101	TS	BF#2	✓		FS	Link
	Pacal et al. [130]	CIBM'22	improved YOLOv3 [121]/v4 [120]	SUN, PL	SUN, PL, ETIS	CDN-53/DN-53	OS	BF#1	✓		FS	Link
	SMPT++ [131]	TMI'22	source-free domain adaptation	Private, C6, ETIS, ASEI, KID	Private, C6, ETIS, ASEI, KID	R-101	OS	BF#1	✓		US	Link
	FRCNN-AA-CIF [132]	CIBM'23	attention module & context information fusion	Private	Private	R-101	TS	BF#1	✓		FS	-
	Haugland et al. [133]	MI'23	modality translation	Private, PL, CDS	PL, KUMC	EffDet-D0	TS	BF#2	✓		FS	-
	SCAN++ [134]	TMM'23	enhanced semantic conditioned adaptation	C6, ASEI	C6, ASEI	R-101	OS	BF#2			FS, US	Link
	TFCNet [135]	CIBM'24	fine-grained feature compensation	C6, KUMC, LDPV	C6, KUMC, LDPV, KSe	CDN-53	OS	BF#1			FS	-
	DUT [136]	TNNLS'24	decoupled unbiased teacher	C6, ASEI, Private	ASEI, Private	R-101	OS	BF#1			US	Link
Video-based models	Tajbakhsh et al. [137]	IPMI'15	patch descriptor & edge classification	Private	Private	AlexNet	TS	BF#1		✓	FS	-
	Tajbakhsh et al. [22]	TMI'15	extension on [137]	C3	C3, ASU	AlexNet	TS	BF#1		✓	FS	-
	Yu et al. [138]	JBHI'16	online and offline integration	ASU	ASU	Customised	OS	MF#2			FS	-
	Mo et al. [139]	ICPR'18	building upon Faster R-CNN [140]	CDB	C6, C3, CDB, ES	V-16	TS	BF#1	✓		FS	-
	Qadir et al. [141]	JBHI'19	temporal dependency	ASU, C6	ASU, CDB	V-16	TS	BF#1	✓		FS	-
	AIPDT [142]	MICCAI'20	parallel detection and tracking	Private, CDB	CDB	DN-53, AlexNet	OS	BF#2			FS	-
	AI-doscopist [42]	NPJDM'20	spatial-temporal fusion	C6, ETIS, C3, ASU, CU, ACP	C6, ETIS, C3, ASU, CU, ACP	R-50	OS	BF#2	✓		FS	-
	STFT [143]	MICCAI'21	spatial-temporal feature transformation	ASU, CDB	ASU, CDB	R-50	OS	BF#2			FS	Link
	Yu et al. [144]	AIM'22	instance tracking head (plug-and-play)	Private, C6, CDB	Private, CDB, ETIS	V-16	OS	BF#2	✓		FS	-
	EMSEN [145]	TII'22	explainable multitask Shapley explanation	CDS	CDS	Customised	OS	BF#2			FS	-
	YONA [146]	MICCAI'23	feature alignment & contrastive learning	SUN, CDB, LDPV	SUN, CDB, LDPV	R-50	TS	BF#2	✓		FS	Link
	Intrator et al. [147]	MICCAI'23	self-supervised polyp re-identification	Private	Private	R-50v2	OS	MF#2			US	-
	V2I-DETR [148]	arXiv'24	video-to-image knowledge distillation	SUN	SUN	R-50	OS	BF#2			FS	-

their processing stages. The two-stage workflow decouples detection into the region proposal and classification phases, like models [127], [132], [139], [141] based on Faster R-CNN [140]. One-stage models prioritise speed and simplicity, operating in a single forward. For example, some studies [42], [130], [142] are based on the YOLO framework [120], [121], and Yu et al. [144] uses the SSD framework [151]. *(c) Architecture:* Detection models predict target categories and spatial coordinates, typically implemented in branched frameworks (BF#1/BF#2) as shown in Fig. 3. Two special cases [128], [138] adapt the design of multistream framework to first pop out pixel-wise attention regions, then convert them to bounding boxes.

• **Output phase.** *(a) Post-processing techniques* are employed to eliminate duplicate predictions and select the most relevant targets, with non-maximum suppression (NMS) being a widely-adopted method [42], [130]–[133], [139], [141], [144], [146]. *(b) Auxiliary information* can improve prediction reliability, such as edge cues suggested to provide geometric patterns for object detection in [22], [128], [137]. *(c) Supervision strategy* is currently dominated by fully supervised learning, such as using region-level labels [126], [130], [132], [133], [139], [141]–[145], [148] and pixel-wise [22], [128], [137], [138] labels, and introducing the box-assisted contrastive learning [146]. Other models [127], [131], [134], [136] explore unsupervised domain adaptation techniques to detect polyps across colonoscopy devices.

• **Remarks.** We emphasise a few observations for the above review. *(a)* Most models focus on detecting polyp(s), while other colonoscopic findings receive less attention. We encourage exploring public multitarget [34] or multicentre [78] data. *(b)* Learning strategies are underexplored. General-purpose detection models like using weak supervision [255] provide valuable references, being potentially more feasible and cost-effective since they require less detailed annotations from medical experts. *(c)* Beyond well-established convolution-based detection frameworks, recent methods like transformer-based DETR [256] and diffusion-based DiffusionDet [257], open exciting opportunities for

this field. Moreover, exploring cross-task synergy is promising, as three video-based models [142], [144], [147] demonstrated effectiveness in unifying polyp detection and tracking frameworks. *(d)* Although some datasets such as the SUN-database [54] (>158K samples) and LDPolyVideo [48] (>900K samples) are relatively large, this field still lacks a standardised evaluation benchmark.

4.3 Segmentation models

Compared to the above two topics, the segmentation research appears to be well established. This is evidenced by the extensive amount of research documented in Tab. 4.

• **Input phase.** Most segmentation models focus on a single target (*i.e.*, polyp), typically adopting as binary segmentation paradigm. These models usually follow the well-established testbed of PraNet [175] for their development and comparison. An exception case, AFP-Mask [196], provides an anchor-free framework for segmenting polyp instances. Recent works [208], [217], [230] have also focused on segmenting surgical tools during procedures.

• **Processing phase.** *(a) Backbone:* The visual encoders for the segmentation task have been extensively explored. A common option is to use a general backbone pre-trained on ImageNet [3], such as using CNN [175], [214], vision Transformer [205], [215], hybrid CNN-Transformer network [186], [193], [223], multilayer perceptron [199], state space model [220], [238], [239], [253], receptance weighted key value (RWKV) [224], and Kolmogorov-Arnold network [224]. An alternative is to use well-trained perception models such as Point DETR [162] used in [209], DeepLab series [157], [167] applied in [189], [233], [234]. Recently, there has been a shift towards promptable architectures. The first way is to exploit the foundation models, for example, by fine-tuning the segment anything modal (SAM) [165] with location prompts [232], adapting SAM during the test time [217], exploiting the hybrid CNN-Transformer network [219], or incorporating trainable adapter layers into the SAM2's encoder [240]. Another way aims to adapt the model to unseen

TABLE 4
Summary of segmentation models in colonoscopy. <u>Dataset:</u> C6 [21], ES [30], KS=Kvasir-SEG [38], C3 [19], ETIS [20], HK [43], ASU [22], CDB [27], BKAI=BKAI-Small [46], KSe [55], GI=GIANA [152], SUN-S [62], PG=PolypGen [69], K-I=Kvasir-Instrument [50]. <u>Backbone:</u> ResUNet [153], R-18/-34/-50/-101 [99], R-50v2 [125], R2-50=Res2Net-50 [154], V-16 [124], DeiT [155], Eff-B4= EfficientNet-B4 [156], DLV3+=DeepLab V3+ [157], PB2/3/5=PVTv2-B2/-B3/-B5 [158], CvT [159], MiT-B2 [160], CMLP=CycleMLP [161], P-DETR=Point DETR [162], D-121=DenseNet121 [98], MN= MSCAN [163], Swin-T [164], SAM [165], SAM2 [166], ViT-B16 [100], DLV2=DeepLabV2 [167], HR-W48=HRNet-W48 [168], CN-T=ConvNeXt-Tiny [169], SFB3=SegFormer-B3 [160], M2Former=Mask2Former [170]. <u>Edge</u>-sensitive analysis by explicitly (EX) using edge map as supervision or input and implicitly exploring edge-aware representation (IM#1) or edge-aware uncertainty (IM#2).

	Model	Publication	Core design	Training dataset	Testing dataset	Backbone	Arch	Edge	Sup	URL
Image-based models	Yuan *et al.* [171]	JBHI'17	weak bottom-up & strong top-down saliency	Private	C6	Customised	BF#1	-	US	
	SFA [172]	MICCAI'19	area & boundary constraints	ES	ES	Customised	BF#1	EX	FS	Link
	ResUNet++ [173]	ISM'19	enhanced deep residual UNet [153]	C6, KS	C6, KS	ResUNet	MF#1	-	FS	Link
	ACSNet [174]	MICCAI'20	adaptive context selection	ES, KS	ES, KS	R-34	BF#1	-	FS	Link
	PraNet [175]	MICCAI'20	reverse attention, parallel partial decoder	C6, KS	C6, ES, KS, C3, ETIS	R2-50	BF#1	EX, IM#1	FS	Link
	UI-CNN [176]	MedIA'20	Monte Carlo guided back-propagation	ES	ES	V-16	MF#1	IM#2	FS	
	ThresholdNet [44]	TMI'20	confidence-guided manifold mixup	ES	ES, WCE-Polyp [44]	R-101	BF#2	EX, IM#1	FS	Link
	SCR-Net [177]	AAAI'21	semantic calibration & refinement	KS	KS	Customised	MF#1	-	FS	
	BI-GCN [178]	BMVC'21	boundary-aware graph convolution	C6, KS	C6, ES, KS, C3, ETIS	R2-50	BF#1	EX	FS	Link
	FDSemi [179]	ICCV'21	collaborative & adversarial learning	C6, KS	C6, KS	Customised	BF#2	IM#1	SS	Link
	CCBANet [180]	MICCAI'21	cascading context & balancing attention	C6, KS	C6, ES, KS	R-34	BF#1	IM#1	FS	Link
	CCD [181]	MICCAI'21	constrained contrastive distribution learning	HK, Liu *et al.* [37]	HK, Liu *et al.* [37]	R-18	BF#2	-	US	Link
	HRENet [182]	MICCAI'21	hard region enhancement	C6, KS	C6, KS, C3	R-34	BF#1	EX	FS	Link
	LOD-Net [183]	MICCAI'21	learnable oriented derivatives	C6, KS	C6, ES, KS, C3, ETIS	R-50	MF#2	EX	FS	Link
	MSNet [184]	MICCAI'21	multiscale subtraction network	C6, KS	C6, ES, KS, C3, ETIS	R2-50	MF#1	EX, IM#1	FS	Link
	SANet [185]	MICCAI'21	colour exchange & probability correction	C6, KS	C6, ES, KS, C3, ETIS	R2-50	MF#2	-	FS	Link
	Transfuse [186]	MICCAI'21	fusing transformers and CNNs	C6, KS	C6, ES, KS, C3, ETIS	R-50v2, ViT-B16	BF#2	EX	FS	Link
	EndoUDA [49]	MICCAI'21	domain adaptation, variational autoencoder training	Celik *et al.* [49]	Celik *et al.* [49]	Eff-B4	BF#2	EX	FS, US	Link
	UACANet [187]	MM'21	uncertainty augmented context attention	C6, KS	C6, ES, KS, C3, ETIS	R2-50	BF#1	EX, IM#2	FS	Link
	Jha *et al.* [55]	JBHI'21	ResUNet++ [173] with conditional random field & test-time augmentation	C6, C3, ETIS, KS, ASU, CDB	C6, C3, ETIS, KS, ASU, CDB	ResUNet	MF#1	-	FS	Link
	MPA-DA [188]	JBHI'21	mutual-prototype adaptation network	ES, KS	ETIS	R-101	BF#2	IM#2	FS, US	Link
	DW-HieraSeg [189]	MedIA'21	hierarchical segmentation, dynamic-weighting	ES	ES	DLV3+	BF#1	-	FS	Link
	ICGNet [190]	IJCAI'22	context-based reverse-contour guidance	ES, KS	ES, C3, KS	R-34	BF#1	EX	FS	-
	BoxPolyp [191]	MICCAI'22	segmentation with extra box labels	C6, KS	C6, ES, KS, C3, ETIS	R2-50, PB2	BF#1	-	WS	Link
	LDNet [192]	MICCAI'22	dynamic kernel generation & update	Private, C6, KS	Private, C6, KS, C3, ETIS	R2-50	BF#1	-	FS	Link
	PPFormer [193]	MICCAI'22	polyp-guided self-attention, local-to-global method	C6, KS	C6, ES, KS, C3, ETIS	V-16, CvT	BF#1	EX	FS	
	SSFormer [194]	MICCAI'22	stepwise local & global feature aggregation	C6, KS	C6, ES, KS, C3, ETIS, KS	MiT-B2	MF#1	-	FS	Link
	TRFR-Net [195]	MICCAI'22	task-relevant feature replenishment	C3, ETIS, KS	C3, ETIS, KS	R-34	BF#2	-	FS, US	Link
	AFP-Mask [196]	JBHI'22	anchor-free instance segmentation	Private, GI	Private, C6, ETIS	Customised	BF#1	-	FS	
	BCNet [197]	JBHI'22	cross-layer integration, bilateral boundary extraction	KS	C6, ES, KS	R2-50	BF#1	EX	FS	Link
	BSCA-Net [198]	PR'22	bit slice context attention	C6, KS	C6, ES, KS, C3, ETIS	R2-50	BF#1	EX	FS	
	Polyp-Mixer [199]	TCSVT'22	context-aware MLP-based network	C6, KS	C6, ES, KS, C3, ETIS	CMLP	BF#1	-	FS	
	ACL-Net [200]	AAAI'23	affinity contrastive learning	C6, KS	C6, ES, KS, C3, ETIS	R-50	BF#2	-	SS	
	WS-DefSegNet [67]	CVPRw'23	deformable transformer, sparse foreground loss	W-Polyp [67]	C6, KS, C3, ETIS, ES	R2-50	MF#2	-	WS, SS	Link
	WeakPolyp [201]	MICCAI'23	mask-to-box transformation, scale consistency	SUN-S, Private	SUN-S, Private	PB2	BF#1	-	WS	Link
	PETNet [202]	MICCAI'23	Gaussian-probabilistic guided semantic fusion	C6, KS	C6, ES, KS, C3, ETIS	PB2	BF#1	-	FS	
	S²ME [203]	MICCAI'23	spatial-spectral mutual teaching, ensemble learning	SUN-S	C6, KS, SUN-S, PG	Customised	BF#1	-	WS	Link
	Su *et al.* [204]	MICCAI'23	feature propagation & aggregation	C6, KS	C6, ES, KS, C3, ETIS	PB2	BF#1	EX	FS	-
	Polyp-PVT [205]	AIR'23	Improved pyramid vision transformer	C6, KS	C6, ES, KS, C3, ETIS	PB2	BF#1	EX	FS	Link
	RPANet [206]	IPMI'23	coarse-to-fine self-supervision	Private	C6, ETIS, KS	R-101	BF#2	-	FS, US	
	FEGNet [207]	JBHI'23	feedback enhancement gate network	C6, KS	C6, ES, KS, C3, ETIS	R2-50	BF#1	EX	FS	
	BS-Loss [208]	JBHI'23	boundary-sensitive loss with location constraint	K-I	K-I	Customised	MF#1	EX	FS	Link
	Point SEGTR [209]	MedIA'23	multi-point and symmetric consistency	C6, ETIS	C6, ETIS	P-DETR	BF#2	-	FS, WS, SS	-
	DGNet [210]	MIR'23	deep gradient learning	C6, KS	C3, ETIS	Eff-B4	BF#1	EX	FS	Link
	CFA-Net [211]	PR'23	cross-level feature fusion, boundary aggregation	C6, KS	C6, ES, KS, C3, ETIS	R2-50	BF#1	EX	FS	Link
	ColnNet [212]	TMI'23	statistical attention, anomaly boundary approximation	C6, KS	C6, ES, KS, C3, ETIS	D-121	BF#1	EX	FS	-
	FANet [213]	TNNLS'23	feedback attention, run-length encoding	C6, KS	C6, KS	Customised	MF#2	-	FS	Link
	MCANet [214]	arXiv'23	multi-scale cross-axis attention	C6, KS	C6, ES, KS, C3, ETIS	MN	MF#1	-	FS	Link
	Polyper [215]	AAAI'24	boundary sensitive attention	C6, KS	C6, KS, C3, ETIS, ES	Swin-T	MF#1	IM#1	FS	Link
	EMCAD [216]	CVPR'24	efficient multi-scale convolutional attention decoding	C6, C3, ETIS, KS, BKAI	C6, C3, ETIS, KS, BKAI	PB2	BF#1	-	FS	Link
	Schön *et al.* [217]	CVPR'24	SAM [165], test-time adaptation	K-I, CDB, KS	K-I, CDB, KS	SAM	BF#2	EX	WS	-
	MH-pFLID [218]	ICML'24	federated learning, injection-distillation paradigm	Private	Private	Customised	BF#2	-	FS	Link
	ASPS [219]	MICCAI'24	SAM [165], uncertainty-guided regularisation	C6, KS	C6, ES, KS, C3, ETIS	SAM, MN	BF#2	IM#2	FS	Link
	Polyp-Mamba [220]	MICCAI'24	vision state space model, semantic relationship mining	C6, KS	C6, ES, KS, C3, ETIS	VMamba [221]	MF#1	EX	FS	-
	QueryNet [222]	MICCAI'24	unified framework of segmentation & detection	C6, KS	C6, ES, KS, C3, ETIS	M2Former	MF#2	-	FS	-
	LSSNet [223]	MICCAI'24	local & shallow feature supplementation	C6, KS	C6, ES, KS, C3, ETIS	PB2	BF#1	EX	FS	Link
	BSBP-RWKV [224]	MM'24	Perona-Malik diffusion, RWKV [225]	KS	KS	Customised	BF#1	EX	FS	-
	CFATransUnet [226]	CIBM'24	channel-wise cross fusion attention and transformer	C6, KS	C6, KS	PB3	BF#1	-	FS	Link
	PolypMixNet [227]	CIBM'24	consistency regularisation, soft pseudo labeling	C3, C6, KS, ETIS	C3, C6, KS, ETIS	R-34	BF#2	-	SS	Link
	RGIAug [228]	JBHI'24	randomised global illumination augmentation	C3, C6, ETIS, KS	C3, C6, ETIS, KS	Customised	BF#2	-	FS	Link
	EMTS-Net [229]	JBHI'24	multi-task synergetic network	C6, KS	C6, ES, KS, C3, ETIS	R2-50	BF#1	-	FS	-
	MSDE-Net [230]	JBHI'24	multi-scale dual-encoding network	K-I	K-I	R-34, DeiT	MF#2	-	FS	-
	Polyp-OOD [231]	MIR'24	out-of-distribution modelling, latent standardisation	SUN-S	SUN-S, C6, C3, ETIS, KS	ViT-B16	MF#2	-	US	Link
	MedSAM [232]	NComs'24	SAM [165], cross-organ/modality tuning	Hybrid datasets	Hybrid datasets	SAM	MF#2	-	WS	Link
	FoBS [233]	TCSVT'24	multi-level boundary-enhanced framework	KS, ES	KS, ES, ETIS, C3	DLV3+	BF#2	EX, IM#1	FS	-
	DCL-PS [234]	TMI'24	domain-interactive contrastive learning, self-training	ETIS, HK, ES, KS	ES, KS	DLV2	BF#2	-	FS, US	Link
	Gao *et al.* [235]	TMI'24	in-context learning, dual similarity checkup	C3	C3	SAM	BF#2	-	WS	-
	U-KAN [236]	arXiv'24	U-shaped Kolmogorov-Arnold network [237]	C6	C6	Customised	MF#1	-	FS	Link
	SliceMamba [238]	arXiv'24	vision state space model, bidirectional slice scan	C6, KS	C6, KS	Customised	MF#1	-	FS	-
	ProMamba [239]	arXiv'24	vision state space model, promptable segmentation	C6, KS	C6, KS, C3, ETIS, ES, BKAI	Vim [149]	MF#2	-	WS	-
	SAM2-UNet [240]	arXiv'24	SAM2 [166], adapter-based tuning	C6, KS	C6, ES, KS, C3, ETIS	SAM2	BF#2	EX	FS	Link
Video-based models	Puyal *et al.* [241]	MICCAI'20	temporal correlation via hybrid 2D/3D CNNs	Private, KS	Private	R-101	MF#2	-	FS	-
	PNS-Net [242]	MICCAI'21	normalised self-attention, progressive learning	C6, C3, ASU, KS	C6, C3	R2-50	BF#2	-	FS	Link
	SSTAN [243]	MICCAI'22	spatial-temporal attention	LDPolyVideo [48]	LDPolyVideo [48]	ResUNet	BF#2	-	SS	-
	TCCNet [244]	IJCAI'22	temporal consistency, context-free loss	C6, C3	C6, C3, ETIS	R2-50	BF#2	EX, IM#1	SS	Link
	Puyal *et al.* [245]	MedIA'22	extend [241] with optimal setups	Private, KS	Private, SUN	R-101	BF#2	-	FS	-
	PNS+ [62]	MIR'22	extend [242] with global-to-local learning	SUN-S	SUN-S	R2-50	BF#2	-	FS	Link
	EUVPS [246]	AAAI'24	cross-scale region linking, cross-wise scale alignment	SUN-S, C6	SUN-S, C6	HR-W48	BF#2	-	FS	-
	LGRNet [247]	MICCAI'24	cyclic neighbourhood propagate, Hilbert selective scan	C6, C3, SUN-S	C6, C3, SUN-S	R2-50	BF#2	-	FS	Link
	SALI [248]	MICCAI'24	short-term alignment, long-term interaction module	SUN-S	SUN-S	PB5	BF#2	EX	FS	Link
	Diff-VPS [249]	MICCAI'24	diffusion model, adversarial temporal reasoning	SUN-S	SUN-S	SFB3	BF#2	-	FS, US	Link
	FlowICBNet [250]	CIBM'24	iterative feedback units, frame filtering & selecting	SUN-S	SUN-S	R2-50	BF#2	-	FS	Link
	Drag&Drop [251]	MIR'24	weakly-supervised temporal annotator	SUN-S	SUN-S	-	BF#2	-	WS	Link
	SSTFB [252]	arXiv'24	self-supervised encoder, sub-branching mechanism	SUN-S	SUN-S, CDB	R2-50	BF#2	-	US, FS	-
	Vivim [253]	arXiv'24	video state space model, spatio-temporal selective scan	KS, ASU, C3, C6	C3, C6	Customised	BF#2	EX	FS	Link
	MAST [254]	arXiv'24	Siamese transformer, mixture attention module	SUN-S	SUN-S	PB2	BF#2	-	FS	Link

scenarios through in-context learning [235]. *(b) Architecture:* The community favours the encoder-decoder design for its superior ability to perceive hierarchical features. Current models usually opt for multistream or branched frameworks, as in Fig. 3. Various modifications in this area have been explored, such as incorporating residual connected flows [55], [173], probing cross-task synergy [222], providing additional edge cues [210], using the model-ensembling strategy [186], [193], [219], calculating latent statistics [231], exploring spatio-temporal relationships through 3D con-

TABLE 5
Comparison of image polyp segmentation models. They are evaluated using the mean scores (%) of structure measure ($\mathcal{S}$ [258]) and Dice coefficient ($\mathcal{D}$) on two test sets, with boxplots illustrating the distribution of their consistency and variability across test cases.

	Kvasir-SEG (100 test images) [38]						CVC-ClinicDB (62 test images) [21]					
Model	$\mathcal{S}$ [#Rank]	0.0 → 0.5 → 1.0	$\mathcal{D}$ [#Rank]	0.0 → 0.5 → 1.0			$\mathcal{S}$ [#Rank]	0.0 → 0.5 → 1.0	$\mathcal{D}$ [#Rank]	0.0 → 0.5 → 1.0		
Polyp-PVT [205]	92.51 [#1]		91.74 [#2]				95.00 [#2]		93.68 [#1]			
CFA-Net [211]	92.40 [#2]		91.47 [#4]				95.07 [#1]		93.25 [#2]			
MSNet [184]	92.31 [#3]		90.23 [#7]				94.68 [#3]		91.48 [#6]			
BoxPolyp [191]	92.30 [#4]		91.84 [#1]				93.70 [#6]		91.81 [#4]			
SSFormer [194]	92.21 [#5]		91.71 [#3]				92.87 [#9]		90.60 [#7]			
UACANet [187]	91.67 [#6]		91.21 [#5]				94.30 [#4]		92.63 [#3]			
PraNet [175]	91.50 [#7]		89.82 [#8]				93.68 [#7]		89.90 [#9]			
SANet [185]	91.45 [#8]		90.41 [#6]				93.98 [#5]		91.57 [#5]			
DGNet [210]	90.98 [#9]		89.72 [#9]				93.39 [#8]		90.44 [#8]			
MCANet [214]	90.25 [#10]		89.55 [#10]				91.79 [#10]		89.70 [#10]			
Polyper [215]	90.08 [#11]		89.12 [#11]				91.29 [#11]		88.63 [#11]			
UNet++ [259]	86.21 [#12]		82.08 [#12]				87.33 [#13]		79.42 [#13]			
UNet [260]	85.76 [#13]		81.83 [#13]				89.00 [#12]		82.25 [#12]			
SFA [172]	78.14 [#14]		72.31 [#14]				79.33 [#14]		70.06 [#14]			

volutions [241], [245] or self-attention modules [62], [242], [248], and approaching with the teacher-student paradigm [67], [209]. *(c) Edge-sensitive analysis:* Geometric patterns are beneficial in enhancing the model's capability to differentiate foreground objects from the background. The current techniques are in two main ways. The first involves the explicit use of edge maps derived from image gradients, either for direct supervision [172], [182], [210] or as an auxiliary input [49]. Moreover, some methods emphasise edge-aware calculation within their loss functions, such as boundary weighted [193], [240] and customised [183], [208]). Second, edge information can be implicitly integrated by embedding edge-aware representations (*e.g.,* reverse attention [175], morphology operator [215], subtraction operator [44]), or by quantifying edge-aware uncertainties [176], [187]. Moreover, some methods adopt a hybrid strategy, *e.g.,* both the subtraction operator and the edge-aware loss are used in MSNet [184].

- **Output phase.** Most models are trained in a fully supervised way, always incorporating deep supervision at various decoding stages, as seen in [175], [205]. Recent models have extended beyond with data-efficient approaches, for example, weakly supervised mask-to-box transformation [201] and unsupervised techniques such as contrastive learning [181], out-of-distribution modelling [231], and pseudo-label supervision [191], [243]. Hybrid supervised strategies are also present in which models [49], [188], [195], [206] undergo fully supervised training in the source domain, and are then adapted to the target domain in an unsupervised way. Point SEGTR [209] exploits three types of supervision to enhance the model. Additionally, some teacher-student networks receive hybrid supervision signals; for example, Ren *et al.* [67] employs a weakly supervised approach for the teacher while the student undergoes semi-supervised training.

- **Remarks.** To reflect current field progress, we analyse 14 open-source image segmentation models on two popular test datasets, as shown in Tab. 5. All models are trained on the same dataset from Fan *et al.*'s benchmark [175]. First, we observe that current learning strategies are underexplored, as evidenced by BoxPolyp, a weakly supervised model obtaining the best $\mathcal{D}$ score (91.84%) on Kvasir-SEG. In addition, some models achieve better performance, yet exhibit wider interquartile ranges in boxplots, indicating their variability

in predictions. For example, Polyp-PVT, which ranks highest in the $\mathcal{S}$ score on Kvasir-SEG, shows a wider interquartile range than other models like SSFormer. From these results, we suggest several promising opportunities for future study. *(a)* The current gold benchmark [175] comprises less than 1.5K samples and is focused on one category (polyp). In general, scaling up both the data size and diversity could be a natural way to improve robustness and generalisability. This demand is driving innovations, such as developing a semi-auto image annotator [165], [166] to reduce expert labour and synthesising high-fidelity content via diffusion [261] and autoregressive [262] techniques. *(b)* Moreover, infinite data scaling is not sustainable. Developing data-efficient strategies [94]–[96] that require fewer or weaker labels is more cost-effective for average users in the community. *(c)* Finally, providing procedural support to physicians is essential, including anomaly detection, navigation planning, risk assessment, and intervention advice. We can adopt innovations from similar topics [263].

4.4 VL models

Compared to the above three topics, multimodal research has relatively fewer references. Most existing methods are discriminative models that aim to learn decision boundaries between multimodal inputs. Some studies demonstrate the model's effectiveness in referring segmentation tasks, for example, by incorporating textual attention of lesion attributes (*e.g.,* size and number of polyps) into a U-shaped model [264], a diffusion model [265], or a hybrid network [266]. Other studies [267], [268] have developd prompt engineering pipelines based on well-trained GLIP [269] for polyp detection. Moreover, the SAM is capable of operating in a VL setting, obtaining location prompts from either the image-text activation map [270] or a zero-shot grounding detector [271], [272]. In the MEDVQA-GI competition [65], most solutions are discriminative-based, approaching VL tasks as a classification mapping problem, where predefined labels are assigned to image-text pairs. An alternative is a generative-based solution [273] that adapts a pretrained BLIP-2 model [274] to generate predictions.

- **Remarks.** Two possible reasons might explain the lag in VL research for colonoscopy. *(a) Data-centric issue.* The lack of well-structured and high-quality image-text pairs hinders progress. Future insights can be learnt from existing

(a) Data overview

ColonINST
- 1. Collecting visual data (303,001 colonoscopy images)
- 2. Generating medical captions (128,620 image-caption pairs)
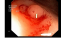- 3. Creating instruction tuning data (450,724 human-machine dialogues)

(b) Data statistic (colonoscopy images)

	Positive	Negative	Total
Train	74,407	106,570	180,977
Val	8,929	17,328	26,257
Test	45,284	50,483	95,767
Total	128,620	174,381	**303,001**

(c) Data taxonomy

(d) Word cloud distribution

(e) Pipeline of caption generation

[*Custom prompt*] You are a specialized caption generator. Carefully examine the provided image and generate a caption of 3 to 5 sentences with a detailed and professional description. The category information of this image is as follows: This is a colonoscopy image of [root], a/an [child] under the category of [parent]. Additional requirements for the generated captions include: 1) Ensure the content is factual and specific to the field. 2) The generated captions must not be broad and must be meaningful.

Category prior
[root] pathological finding
[parent] polyp related
[child] hyperplastic lesion

[*Medical captions*] This endoscopic image reveals a hyperplastic polyp within the gastrointestinal tract, characterized by its **smooth, round, and nodular appearance** typically seen arising from the mucosal layer. The lesion's **surface appears intact without evidence of erosion or ulceration**, which can be distinguishing features of benign hyperplastic polyps versus malignancy. **Surrounding mucosa appears slightly erythematous, but without significant inflammatory changes**, suggesting a localized lesion rather than a diffuse pathological process. The field of view includes normal vascular patterns surrounding the polyp, indicating preserved tissue integrity. This lesion is representative of the most common type of non-neoplastic polyp found in the colon, often identified incidentally during screening colonoscopies.

(f) Data statistic (human-machine dialogues)

	CLS	REG	REC	CAP	Total
Train	74,407	54,237	54,237	74,407	257,288
Val	8,929	4,874	4,874	8,929	27,606
Test	45,284	37,631	37,631	45,284	165,830
Total	128,620	96,742	96,742	128,620	450,724

Fig. 4. **Details of the established ColonINST.** (a) Three sequential steps to create the instruction tuning dataset for multimodal research. (b) Numbers of colonoscopy images designated for training, validation, and testing purposes. (c) Data taxonomy of three-level categories. (d) A word cloud of the category distribution by name size. (e) Caption generation pipeline using the VL prompting mode of GPT-4V [4]. (f) Numbers of human-machine dialogues created for four downstream tasks.

---

ideas. First, crawling unlabelled image-text data from social media [275] and scientific literature [276] can be used to build domain-specific foundation models. Second, language models such as GPT-4V [4] can generate diverse professional descriptions, offering an economical and scalable way to expand the knowledge space of the data. *(b) Model-centric issue.* Current VL techniques in colonoscopy have not kept pace, even with recent developments in multimodal language models (MLMs) [8], [277] for general domains. These techniques opt for a decoder-only strategy that unifies multiple tasks (*e.g.*, detection, captioning) into a unified autoregressive framework (*i.e.*, next-token prediction). These models are flexibly capable of processing input and output texts of varying lengths, without requiring additional task-specific prediction heads for different tasks.

5 STEPPING INTO THE MULTIMODAL LAND

Recently, MLMs have demonstrated significant promise in leveraging language models to process multimodal signals, especially in "perceiving and interpreting" visual signals. Instruction tuning [278] is key to instructing the MLMs to execute domain-specific tasks aligned with user preferences. This section introduces three initiatives to advance multimodal research: how we create a large-scale instruction tuning dataset, ColonINST (§5.1) and how we train a colonoscopy-specific MLM, ColonGPT (§5.2). Finally, as in §5.3, we contribute a multimodal benchmark for conversational colonoscopy tasks, conduct diagnostic studies on ColonGPT, and share lessons from empirical observations.

5.1 Established instruction tuning dataset: ColonINST

● **Overview.** Fig. (4-a) depicts our semi-automated workflow to create instruction tuning data in three steps. We begin by assembling colonoscopy images from public datasets. Following this, we use a category-specific prompt to interact with a multimodal AI chatbot, GPT-4V [4], yielding descriptive medical captions for these positive cases within the assembled data. Lastly, we reorganise the instruction tuning pairs derived from the data afore-prepared, enabling the model to perform four different colonoscopy tasks in an interactive, dialogue-based manner.

● **Data collection.** As shown in Fig. (4-b), ColonINST contains 303,001 colonoscopy images, including 128,620 positive and 174,381 negative cases collected from 19 different data sources. To ensure data integrity and avoid label leakage, we establish a series of management rules to divide each dataset. For datasets with predefined divisions, such as KUMC [57], PICCOLO [39], WCE-CCDD [60], BKAI-Small [46], CP-CHILD [51], Kvasir-Instrument [50], and PS-NBI2K [16], we follow their original division rules. When such predefined rules are not available, we conform to widely recognised benchmarks, such as CVC-ClinicDB [21], CVC-ColonDB [19], ETIS-Larib [20], and the polyp category in Kvasir [28] according to the benchmark by Fan *et al.* [175], as well as positive samples in SUN-database [54] following the benchmark by Ji *et al.* [62]. For the remaining datasets (HyperKvasir [43], Kvasir-Capsule [56], CPC-Paired [47], Nerthus [29], GastroVision [66], EDD2020 [40], PolypGen [69], negative samples in SUN-database [54], remaining categories in Kvasir [28]), we allocate them proportionally as 60%/10%/30% for training/validation/testing purposes. With the above management rules, our final image division for is roughly 59.73%/8.77%/31.61%. As depicted in Fig. (4-c), all images are classified into a three-level structure, including 4 root/13 parent/62 child categories. In detail, the root level contains three positive categories: the pathological findings of various colonic diseases (110,970 cases); the anatomical structure related to the colon (5,511 cases); and therapeutic interventions related to colonoscopy (12,139 cases), covering the pre-operative, intra-operative, and post-operative stages. Targets outside our interest (*e.g.*, stomach, oesophagus, normal Z-line, and gastric polyp not

TABLE 6
Details of instruction tuning dataset ColonINST. For each task, we provide five templates for human instructions, the data sources used to organise human-machine dialogues, and an example of a human-machine conversation.

Task	Instruction templates	Data source	Human-machine dialogue sample
CLS	1. Categorize the object. 2. Determine the object's category. 3. Identify the category of the object. 4. Classify the object's category. 5. Assign the object to its corresponding category.	19 sources → SUN-database [54], PolypGen [69], CVC-ClinicDB [21], ETIS [20], KUMC [57], Kvasir [28], PSNBI2K [16], CVC-ColonDB [19], EDD2020 [40], Kvasir-Capsule [56], CP-CHILD [51], BKAI-Small [46], PICCOLO [39], WCE-CCDD [60], CPC-Paired [47], HyperKvasir [43], Nerthus [29], GastroVision [66], Kvasi-Instrument [50]	*Human:* "Assign the object to its corresponding category" *Answer: "polyp"*
REG	1. What category does {*object coordinates*} belong to? 2. Can you tell me the category of {*object coordinates*}? 3. Could you provide the category for {*object coordinates*}? 4. Please specify the category of {*object coordinates*}. 5. What is the category for {*coordinates*}?	11 sources → SUN-database [54], PolypGen [69], CVC-ClinicDB [21], ETIS [20], KUMC [57], Kvasir [28], PSNBI2K [16], CVC-ColonDB [19], EDD2020 [40], Kvasir-Capsule [56], Kvasi-Instrument [50]	*Human: "Could you provide the category for [<147><317><665><770>]?"* *Answer: "high grade adenoma"*
REC	1. Where is the location of {*object category*}? 2. Could you give the position of {*object category*}? 3. Where is {*category*} located? 4. Could you specify the location of {*object category*}? 5. Please specify the coordinates of {*object category*}.	11 sources → SUN-database [54], PolypGen [69], CVC-ClinicDB [21], ETIS [20], KUMC [57], Kvasir [28], PSNBI2K [16], CVC-ColonDB [19], EDD2020 [40], Kvasir-Capsule [56], Kvasi-Instrument [50]	*Human: "Where is adenomatous located?"* *Answer: "[<128><406><216><496>]"*
CAP	1. Describe what you see in the image. 2. Interpret what the image shows. 3. Detail the visual elements in the image. 4. Explain the image's visuals thoroughly. 5. Offer a thorough explanation of the image.	19 sources → SUN-database [54], PolypGen [69], CVC-ClinicDB [21], ETIS [20], KUMC [57], Kvasir [28], PSNBI2K [16], CVC-ColonDB [19], EDD2020 [40], Kvasir-Capsule [56], CP-CHILD [51], BKAI-Small [46], PICCOLO [39], WCE-CCDD [60], CPC-Paired [47], HyperKvasir [43], Nerthus [29], GastroVision [66], Kvasi-Instrument [50]	*Human: "Detail the visual elements in the image."* *Answer: "The image displays a medical endoscopic view …"*

occurred during a colonoscopy) or lack of objects (*e.g.*, normal mucosa, colon background) are classified under the negative root category (174,381 cases). We intentionally keep these negative samples, as they may be valuable for future gastrointestinal research. Fig. (4-d) presents a word cloud distribution for all categories names within ColonINST.

• **Caption generation.** The behavioural study [279] suggests that language affects both higher-level (recognition) and lower-level (discrimination) processes of visual perception. This encourages us to extend positive cases (*i.e.*, 128,620 images featuring various colonoscopic findings) with descriptive captions. For this purpose, a straightforward way to create captions is to wrap the category name in a basic template, like "a photo of a [category]" as used by Radford *et al.* [150]. However, these simple sentences tend to yield suboptimal multimodal alignment, as they are less informative. As shown in Fig. (4-e), we introduce a pipeline to generate more descriptive captions. We interact with GPT-4V [4] using a custom prompt for each colonoscopy image. These prompts act as a prior, conditioned by the image's category. Compared to simple sentences, the generated captions explain three features. First, our generated captions describe the unique patterns of the target, such as "smooth, round, and nodular appearance", providing details of the surface of the object. Second, conditioned by category priors, our captions can better differentiate between benign hyperplastic polyps and malignant lesions, describing lesion as "surface appears intact without evidence of erosion or ulceration". Third, our captions cover not only the lesion itself but also the surroundings, *e.g.*, "mucosa appears slightly erythematous, but without significant inflammatory changes", offering a more holistic and accurate interpretation.

• **Organising tuning data.** In the final step, we convert all positive cases into a one-round conversational format, *i.e.*, "image+human instruction→machine response". As depicted in Fig. (4-f), we reorganise 450,724 human-machine dialogue pairs from various image/label/caption sources, covering four different tasks. Specifically, the classification task (CLS) requires the model to assign a category tag to a colonoscopy image. Using the localisation labels, we introduce two related tasks: referring expression generation (REG), which involves classifying a specified image region, and referring expression comprehension (REC), which in-
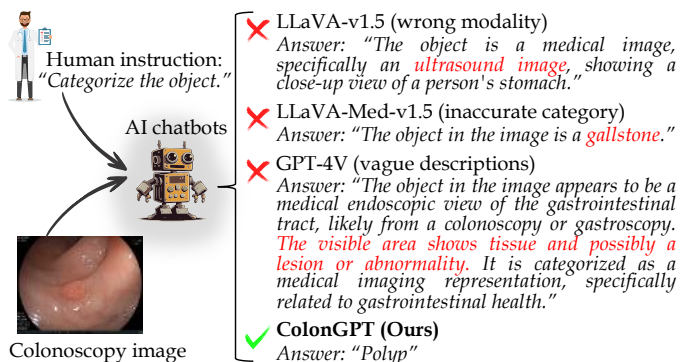

Fig. 5. **Response comparison for colonoscopy image classification.** We evaluate the zero-shot language responses from three AI chatbots against the response from our multimodal model, ColonGPT.

volves locating an object with the given category. We also introduce the image captioning (CAP) task that uses GPT-4V-generated captions as machine responses. To enhance dialogue diversity, we set up five question templates per task, in which we randomly select one to form a human-machine instruction pair, explained in Tab. 6.

5.2 Proposed multimodal language model: ColonGPT

• **Motivation.** As illustrated in Fig. 5, three AI chatbots – LLaVA-v1.5 [8], LLaVA-Med-v1.5 [280], and GPT-4V [4] – are evaluated for their zero-shot language response capabilities. They often produce inaccurate or vague responses and cannot be readily adaptable to specific colonoscopy tasks. This motivates us to develop a colonoscopy-specific MLM for the community. As a result, ColonGPT classifies the image as "polyp" according to the user instructions, allowing for more precise and personalised applications.

• **Overview.** We strive to verify the efficacy of language models (LMs) in interpreting both visual and textual signals within the field of medical optical imaging. We present a baseline model, called ColonGPT, to execute colonoscopy tasks following human instructions. As shown in the left of Fig. 6, we follow the framework of MLM [8], which typically involves four basic components. *(a)* A language tokenizer translates a human instruction $\mathbf{X}_q$ into a sequence of tokens $\mathbf{T}_q \in \mathbb{R}^{N_q \times D}$, where N_q signifies the length of textual tokens and D represents the embedding dimension. *(b)* A visual
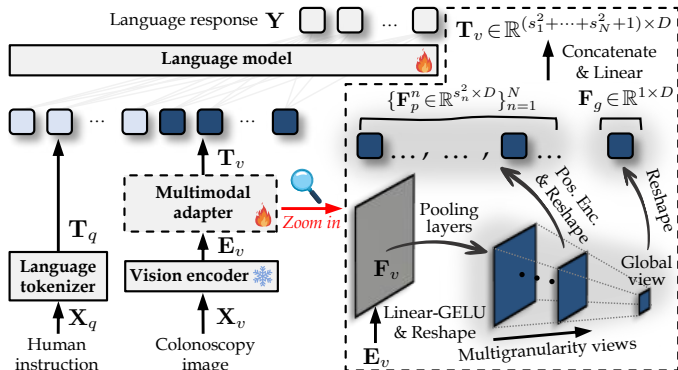
Fig. 6. **Details of our multimodal language model, ColonGPT.**

encoder, typically based on a transformer, condenses a colonoscopy image $\mathbf{X}_v \in \mathbb{R}^{H \times W \times 3}$, with height H and width W, into a flattend visual embedding $\mathbf{E}_v \in \mathbb{R}^{\frac{HW}{P^2} \times d}$. Here, P denotes the patch size and d refers to the token dimension. *(c)* A multimodal adapter transforms the visual embedding $\mathbf{E}_v$ into N_v numeric tokens $\mathbf{T}_v \in \mathbb{R}^{N_v \times D}$, matching the language dimension D with $\mathbf{T}_q$. *(d)* Finally, a language model receives the concatenated visual tokens $\mathbf{T}_v$ and text tokens $\mathbf{T}_q$ as input. Using the chain rule of probability, a sequence $\mathbf{Y}$ of length L is generated in an autoregressive way, formulated as $p(\mathbf{Y}) = \prod_{i=1}^{L} p(y_i \mid \mathbf{T}_v, \mathbf{T}_q, \mathbf{Y}_{<i})$, where $\mathbf{Y}_{<i} = [y_1, y_2, \cdots, y_{i-1}]$ is the sequence of predicted language tokens indexed before i.

● **Multigranularity multimodal adapter.** Previous works [7]–[9] generally employ a multilayer perceptron architecture as a multimodal adapter, typically consisting of triple linear layers with intervening GELUs. However, handling all visual tokens introduces redundancy because not every token is equally significant, and it also incurs higher computational costs given the quadratic complexity in relation to the number of input tokens. To embrace these challenges, we propose a multimodal adapter that incorporates multigranularity pooling layers between two linear layers. As illustrated in the right of Fig. 6, we transform the embedding $\mathbf{E}_v \in \mathbb{R}^{\frac{HW}{P^2} \times d}$ from d-dim to D-dim using a linear layer followed by a GELU, then reshape it into the spatial format $\mathbf{F}_v \in \mathbb{R}^{\frac{H}{P} \times \frac{W}{P} \times D}$. To reduce the number of visual tokens while avoiding performance drops, we roll out three modifications for the pooling phase, each validated in §5.3.2. *(a) Multigranularity views.* We add a set of adaptive average pooling operations with N kernel sizes $\{s_1, \ldots, s_N\}$ to obtain multigranularity features. In particular, this adaptive operator accommodates input sequences of varying lengths, *i.e.*, the pooled feature for the kernel size s_n is shaped as $\mathbb{R}^{s_n \times s_n \times D}$. *(b) Positional encoding.* Inspired by [281], we enhance the spatial information within each pooled feature by applying a 2D convolutional layer with the appropriate zero-padding setting. By default, a zero-pixel boundary is added around the input feature. *(c) Global view.* We also use a global average pooling layer with kernel size 1 on the feature $\mathbf{F}_v$ to obtain a global view with the shape of $\mathbb{R}^{1 \times 1 \times D}$. Lastly, we reshape each pooled feature into flattened vectors: $\{\mathbf{F}_p^n \in \mathbb{R}^{s_n^2 \times D}\}_{n=1}^N$ and $\mathbf{F}_g \in \mathbb{R}^{1 \times D}$. We concatenate these vectors and process the resulting vector through the second linear layer to produce the final visual

tokens $\mathbf{T}_v \in \mathbb{R}^{N_v \times D}$, where $N_v = (s_1^2 + \cdots + s_N^2 + 1)$ denotes the length of the visual tokens.

● **Implementation.** Our model can be integrated with modern off-the-shelf visual encoders and LMs. To improve reproducibility for average users, we implement ColonGPT in an resource-friendly way. First, we employ SigLIP-SO (0.4B parameters) [5] as the visual encoder, with an input resolution of $H = W = 384$, a patch size of $P = 14$, and a visual embedding dimension of $d = 1152$. This configuration yields a visual embedding $\mathbf{E}_v$ with a shape $\mathbb{R}^{729 \times 1152}$, where the number of visual tokens is $729 = \lfloor \frac{384}{14} \rfloor^2$. In addition, Phi-1.5 (1.3B parameters) [6] serves as the language tokenizer and language model, with a embedding size of $D = 2048$. To reduce computational cost, the size of pooling kernels is set to $\{s_1, s_2\} = \{14, 7\}$, significantly reducing the visual tokens N_v from 729 to 246, a reduction of 66.26%. This design allows us to complete training in five hours, facilitating rapid proof-of-concept development.

● **Training recipe.** We implement our model using PyTorch library, accelerated by four NVIDIA A100-40GB GPUs. The AdamW optimiser is used with an initial learning rate of 2e-3 and a cosine learning rate scheduler. Our ColonGPT is trained on the combination of training and validation dialogues from ColonINST. The complete training runs for three epochs, with a batch size of 16 per GPU and a gradient accumulation every 2 steps. During training, the visual encoder is frozen, focusing on the trainable multimodal adapter and the LM. For efficiency, we utilise the low-rank adaptation (LoRA [282]) strategy for LM, with a rank of $r = 128$ and a scaling factor of $\alpha = 256$.

5.3 Experiments

5.3.1 Multimodal benchmark

● **Model competitors.** To establish a widely accepted multimodal benchmark for the community, we select eight popular MLMs as competitors, including six general-purpose and two medically tailored models. As shown in Tab. 7, each competitor has two training setups depending on whether it uses LoRA [282] or initialises knowledge from additional pre-training data. We retrain all competitors using the combined training and validation dialogues from ColonINST, as used in our ColonGPT.

● **Evaluation protocols.** We quantitatively evaluate three conversational tasks for the multimodal benchmark. For the two classification-based tasks, namely CLS and REG, we adopt the accuracy metric ($\mathcal{A}$) to calculate the ratio of correctly predicted categories to the total number of predictions. For the REC task, we use the intersection over union (IoU) metric to measure the localisation precision. Furthermore, due to the subjective nature of language in the CAP task, we qualitatively analyse the medical accuracy of the responses by verifying the correct identification of the anatomical structures and category names visible in the images, or relevant clinical information descriptions.

● **Learning ability.** We begin by conducting an open-book test for each model to quantitatively measure how effectively each model has internalised the visual and linguistic patterns from the training phase. Specifically, we evaluate each model on the samples they have seen during training, *i.e.*, 27,606 validation dialogues. The "*seen*" columns in Tab.

TABLE 7

Multimodal benchmark for three conversational tasks. "LoRA" refers to fine-tuning using low-rank adaptation [282]. "EXT" indicates the use of pre-trained weights on extra data. We compare the results on the seen samples from the validation set and the unseen samples from the testing set of ColonINST. The symbol ↑ signifies that a higher score reflects better performance.

Model	Visual encoder (input shape/URL)	Language model (model size/URL)	No.	LoRA	EXT	CLS task ($\mathcal{A}$ ↑) seen	unseen	REG task ($\mathcal{A}$ ↑) seen	unseen	REC task (IoU ↑) seen	unseen
MiniGPT-v2 [7]	EVA-G/14 (448px/link)	LLaMA2 (7B/link)	#A$_1$	✓		91.49%	77.93%	94.69%	72.05%	23.45%	15.36%
			#A$_2$	✓	✓	90.00%	76.82%	87.65%	70.23%	27.97%	31.13%
LLaVA-v1 [277]	CLIP-L/14 (224px/link)	Vicuna-v1.3 (7B/link)	#B$_1$	✓		87.86%	72.08%	84.55%	68.11%	20.05%	12.72%
			#B$_2$	✓	✓	89.61%	42.17%	86.87%	46.85%	21.81%	3.24%
LLaVA-v1.5 [8]	CLIP-L/14 (336px/link)	Vicuna-v1.5 (7B/link)	#C$_1$	✓		92.97%	79.10%	98.58%	70.38%	55.72%	34.32%
			#C$_2$	✓	✓	93.33%	80.89%	**99.32%**	72.88%	61.97%	42.31%
Bunny-v1.0-3B [9]	SigLIP-SO (384px/link)	Phi2 (2.7B/link)	#D$_1$	✓		91.16%	75.50%	96.61%	69.45%	46.24%	31.24%
			#D$_2$	✓	✓	92.47%	79.50%	96.02%	75.08%	54.00%	41.48%
MGM-2B [283]	CLIP-L/14 (336px/link) & ConvNeXt-L (768px/link)	Gemma (2B/link)	#E$_1$			92.97%	78.99%	98.17%	69.81%	39.78%	16.00%
			#E$_2$		✓	93.24%	78.69%	98.75%	74.30%	57.25%	25.23%
MobileVLM-1.7B [284]	CLIP-L/14 (336px/link)	MobileLLaMA (1.4B/link)	#F$_1$		✓	93.02%	78.75%	97.78%	73.14%	47.30%	31.46%
			#F$_2$	✓	✓	93.64%	80.44%	97.87%	78.03%	51.36%	34.80%
LLaVA-Med-v1.0 [280]	CLIP-L/14 (224px/link)	LLaMA1 (7B/link)	#G$_1$			93.52%	78.04%	97.74%	75.07%	41.60%	24.89%
			#G$_2$		✓	93.84%	77.38%	97.35%	75.25%	39.43%	20.85%
LLaVA-Med-v1.5 [280]	CLIP-L/14 (224px/link)	Mistral-v0.2 (7B/link)	#H$_1$	✓		93.62%	79.24%	99.30%	73.05%	64.69%	41.97%
			#H$_2$	✓	✓	87.22%	66.51%	90.40%	70.00%	13.39%	12.95%
ColonGPT (Ours)	SigLIP-SO (384px/link)	Phi1.5 (1.3B/link)	-	✓		**94.02%**	**85.81%**	99.02%	**83.42%**	**65.89%**	**45.77%**
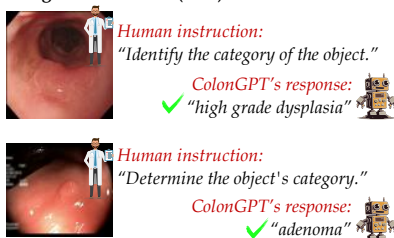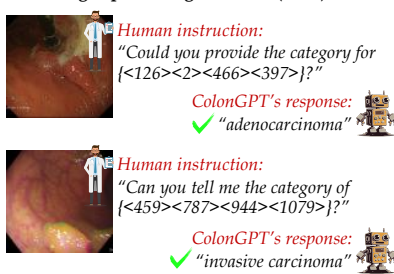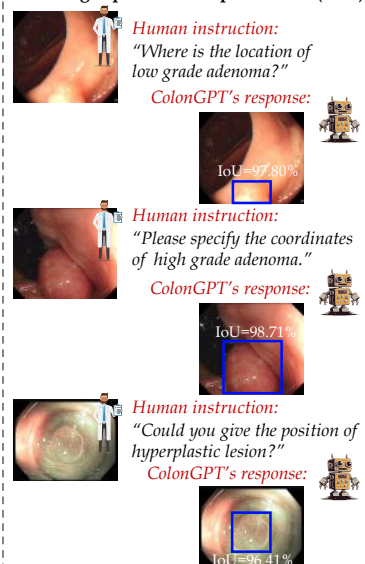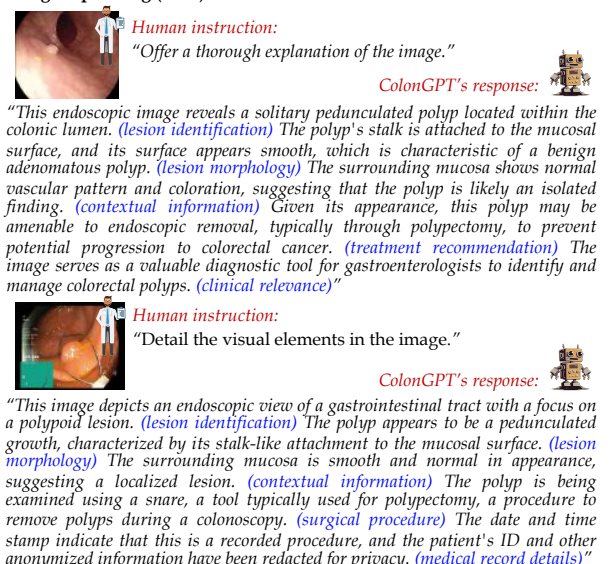
Fig. 7. **Illustration of ColonGPT's multimodal capabilities.** Our model can execute various multimodal colonoscopy tasks through conversational interactions, including comprehension (CLS, REG), localisation (REC), and captioning (CAP) based.

7 show that we achieve the highest scores in the CLS ($\mathcal{A} = 94.02\%$) and REC (IoU $= 65.89\%$) tasks. This implies that ColonGPT has a better learning ability, which allows it to classify images and understand reference expressions related to specific visual regions. Furthermore, we achieve an accuracy of 99.02%, below 99.32% achieved by LLaVA-v1.5 (#C$_2$). This gap ($\Delta = 0.3\%$) is due to a 7B-level LM used in LLaVA-v1.5, which has also been pretrained on additional data and thus gained more knowledge.

• **Generalisation ability.** We further conduct a closed-book test to examine each model's ability to generalise knowledge to unseen conditions, *i.e.*, 165,830 testing samples of ColonINST. The "unseen" columns in Tab. 7 consistently reveal our superior performance in unseen samples in all three tasks. Recall that our model performs worse than LLaVA-v1.5 in the REG task for seen scenarios. However, this gap is overtaken when exposed to unseen scenarios, where we achieve an accuracy of 83.42%, even exceeding the 7B-level LLaVA-v1.5 (#C$_2$) by 10.54%. Compared to the runner-up model, LLaVA-Med-v1.5 (#H$_1$), our model

surpasses it by 1.2% in the seen scenarios for the REC task, and this gap is further widened by 3.8% in the unseen scenarios. These results show the potential of ColonGPT as a conversational assistant for multimodal colonoscopy tasks, especially in generalising to unseen data.

• **Qualitative analysis.** Fig. 7 illustrates our model's three multimodal abilities across four conversational tasks. *(a) Comprehension ability:* In the CLS task, we identify subtle visual features, distinguishing "high grade dysplasia" from "adenoma" in visually similar images. In the REG task, we correctly translate complex visual features from the given coordinates into precise medical terminology. *(b) Localisation ability:* This entails ColonGPT understanding language query and localising visual target within a complex colon environment. The outputs of the REC task showcase ColonGPT's precision in localising specified expressions using bounding boxes. *(c) Captioning ability:* This requires the synthesis of visual information into coherent, clinically relevant text. Our model provides descriptions of a pedunculated polyp, detailing its morphology, contextual characteristics,

TABLE 8
Diagnostic studies of three core components in ColonGPT. "∗": interpolate the position embeddings for higher resolution, specifically from 224px to 384px. Our default configurations are shaded with a gray background.

(a) Different presentations from visual encoder

Visual encoder	input/URL	CLS	REG	REC
ConvNeXtV2-L	384px/link	82.95%	78.63%	33.74%
ViT-L	384px/link	82.16%	77.04%	40.78%
MAE-L*	384px/link	80.85%	75.87%	38.53%
MAE-L	224px/link	81.95%	77.62%	43.25%
DINOv2-L*	384px/link	35.03%	22.91%	6.79%
DINOv2-L	224px/link	21.22%	7.96%	2.69%
CLIP-L	336px/link	83.99%	78.67%	41.54%
SigLIP-SO	384px/link	85.81%	83.42%	45.77%

(b) Multigranuarity multimodal adapter

	token (ratio)	CLS	REG	REC
MLP baseline	729 (100.00%)	83.53%	81.80%	43.70%
{16, 8, 1}	321 (44.03%)	84.39%	80.90%	46.37%
{14, 7, 1}	246 (33.74%)	85.81%	83.42%	45.77%
{12, 6, 1}	181 (24.83%)	83.74%	81.60%	45.94%
{10, 5, 1}	126 (17.28%)	84.28%	82.01%	46.46%
{8, 4, 1}	81 (11.11%)	84.70%	81.36%	45.30%
w/o Pos. Enc.	246 (33.74%)	84.50%	82.91%	40.09%

(c) Fine-tuning strategy

Strategy	r	α	CLS	REG	REC
full-tuning	-	-	78.06%	73.79%	**50.20%**
LoRA	4	8	85.43%	82.75%	45.02%
LoRA	8	16	84.45%	80.78%	44.98%
LoRA	16	32	84.39%	80.81%	45.90%
LoRA	32	64	84.91%	82.73%	45.56%
LoRA	64	128	83.84%	81.19%	43.57%
LoRA	128	256	85.81%	83.42%	45.77%
LoRA	256	512	82.93%	79.96%	48.27%

and potential clinical relevance. Additionally, ColonGPT can describe the treatment procedure when an instrument is present, *e.g.*, "The polyp is being examined using a snare."

5.3.2 Diagnostic studies

• **Visual encoder.** Our diagnostic experiment begins with an inquiry – *What types of visual representations are appropriate for multimodal colonoscopy data?* We prepare four sets of representations from various large-scale pre-training strategies: supervised learning (ConvNeXtV2 [285], ViT [100]), reconstructive learning (MAE [286]), and contrastive learning using vision-only data (DINOv2 [287]) or VL data (CLIP [288], SigLIP [5]). As shown in Tab. (8-a), all encoders use pre-trained weights from Huggingface. To ensure consistency, we manually interpolate the smaller position embedding for MAE and DINOv2 from 224px to 384px (marked with ∗), while leaving the default input of the remaining models unchanged. Our observation reveals that contrastive learning encoders using VL data outperform other strategies. This suggests that visual representations pre-aligned with weak texts during their pre-training facilitate us to transform visual embeddings into the language space. Regarding the other unimodal encoders, both supervised learning methods (ConvNeXtV2, ViT) and the reconstructive approach (MAE) give satisfactory feedback. However, the vision-only contrastive learning model (DINOv2) struggles, especially in the REC and REG tasks. Multiple efforts to optimise DINOv2 with various hyperparameters, including input size, model size, and learning rate, did not produce acceptable results for multimodal colonoscopy tasks.

• **Multigranularity multimodal adapter.** It serves as a key component in linking vision and language modalities, reducing visual tokens to mitigate computational overhead. As detailed in Tab. (8-b), we analyse its effectiveness from three perspectives. *(a) How to configure the pooling kernels?* As a reference, we initialise a baseline variant of ColonGPT with a multimodal adapter used in [7], [8], which employs a pure MLP architecture to process all input tokens equally. We then gradually decrease the size of the pooling kernels across five variants: {16, 8, 1}, {14, 7, 1}, {12, 6, 1}, {10, 5, 1}, and {8, 4, 1}. Concerning the performance-cost trade-offs, our setup {14, 7, 1} is optimal. It decreases the visual tokens from 100% (729 tokens) to 33.74% (246 tokens) while maintaining impressive results across three conversational tasks. To illustrate, we observe performance gains of 2.28%, 1.62%, and 2.07% in the CLS, REG, and REC tasks, respectively. *(b) Is global context necessary?* We remove the global view from our default setup {14, 7, 1} for the multigranularity adapter, producing a controlled variant with setup {14, 7}. The performance then declines, indicating the necessity of

capturing the global context within visual embeddings for improved outcomes. *(c) Is positional encoding important?* As shown in the last row of Tab. (8-b), our setup without positional encoding shows a significant performance drop in REC task, from 45.77% to 40.09%. This suggests that the relative position information for the visual sequence is crucial for the localisation task.

• **Fine-tuning strategy.** Lastly, we investigate *how to effectively tune our model on multimodal colonoscopy data*. As shown in Tab. (8-c), we initiate a set of variants to tune the language model, Phi1.5. It includes seven variants with different setups for LoRA and a full-tuning variant as a reference point. The best performance was observed in the LoRA variant with configuration $r/\alpha = 128/256$, achieving 85.81% and 83.42% in the CLS and REG tasks, respectively. In addition, the other two variants achieve outstanding scores in the REC task, with the full-tuning variant achieving 50.20% and the LoRA with configuration $r/\alpha = 256/512$ reaching 48.27%. This implies that more tunable parameters for the language model could allow ColonGPT to capture more complex patterns in the spatial planes. Therefore, we believe that there remains room to improve the localisation ability of ColonGPT in the REC task, such as increasing the rank factor r and finding a matched scaling factor α. For training efficiency, we finally choose $r/\alpha = 128/256$ as our default configuration, as it allows us to reduce the training time from eight to roughly five hours.

5.3.3 Empirical takeaways

This study represents a preliminary exploration of multimodal instruction tuning techniques in colonoscopy. We unify the multimodal and multitask paradigms in a causal language model, which features two insights: interpreting visual content within the linguistic space and tackling various visual tasks under a next-token prediction framework. We finally derive lessons from experiments that may guide future advances in multimodal research.

• **Embracing data scarcity.** In general, MLMs [8], [277] opt for a two-stage strategy trained on massive data, *e.g.*, ∼558K samples for multimodal alignment, followed by ∼665K instruction tuning samples to ensure human compliance. Alternatively, we adopt a single-stage strategy to directly fine-tune ColonGPT on comparatively smaller training data with ∼285K instructions. This strategy appears to be effective in colonoscopy, a data-limited scenario. We suggest two feasible ways to compensate for this data-centric issue. *(a)* Scaling up data size is a straightforward way to improve the domain-specific representation ability. A cost-efficient way is to consider synthesised data once the public data sources are used up [289]. *(b)* Diversifying

the human-machine dialogue can efficiently train an AI specialist for colonoscopy applications. This involves expanding question-answer pairs with advanced AI chatbots and organising more executable tasks, such as converting masks into polygons for segmentation [290] or modelling multiframe correlations for video analysis [291].

● **Efficiency drives progress.** As discussed above, we take less data to obtain greater performance than other model rivals. This success benefits from the way we build ColonGPT. *(a)* Colonoscopy data inherently contains redundant information, such as the fact that most mucosal surfaces are similar, as well as camouflaged patterns between benign lesions and their surroundings, as discussed in §2.2. To reduce redundancy, we propose a multigranularity multimodal adapter that selectively samples tokens without compromising performance. For future improvement, we can draw on the wisdom of previous token reduction techniques [292]. *(b)* As shown in Tab. 7, the Phi1.5 model [6], although lightweight, shows surprising efficiency, even outperforming other 7B-level competitors. This indicates that larger models appear to require more colonoscopy data. Thus, future efforts should prioritise enhancing training and inference efficiency, especially for the medical field, rather than racing with massive computational resources. A promising idea to streamline the MLM framework using an encoder-free solution [293] to interpret visual pixels.

● **Improving spatial perception.** We observe that the ability to accurately locate targets given descriptions remains limited. This is evident in the REC results shown in Tab. 7, where IoU scores fall below 50% in most models when tested on unseen samples. To break through this performance bottleneck, we suggest two potential routes. *(a)* In constructing ColonGPT, we leverage a pre-trained visual encoder and a language model from the general domain. This approach presents challenges of the gaps between general and medical optical data, as well as the gap between vision and language modalities. As recommended in [294], pre-training and pre-aligning the multimodal space before instruction tuning would be a promising approach to alleviate these issues. *(b)* The next-token prediction framework of causal language models may struggle with arithmetic tasks due to the snowballing error resulting from the chain rule [295]. For example, LMs are not responsible for accurately predicting coordinates in the REC task. We encourage that the vision and language parts of the next-generation framework can handle their respective roles, such as a parallel framework [296] that predicts segmentation masks and generates language captions, simultaneously.

6 CONCLUSION

We investigate the frontiers in intelligent colonoscopy techniques and their broader implications in the multimodal field. Our structure follows two primary threads. First, we survey the landscape of four colonoscopic scene perception tasks and sort out the key challenges and understudied areas. Second, our survey reveals that multimodal research in colonoscopy is underexplored. To embrace this, we contribute three initiatives to the community: a large-scale multimodal instruction tuning dataset ColonINST,

a colonoscopy-specific multimodal language model ColonGPT, and a multimodal benchmark. Importantly, multimodal colonoscopy research is rapidly advancing. Future developments can build on recent breakthroughs, such as executing role-playing tasks with agents [297].

REFERENCES

[1] C. Eng, T. Yoshino, E. Ruíz-García, N. Mostafa, C. G. Cann, B. O'Brian, A. Benny, R. O. Perez, and C. Cremolini, "Colorectal cancer," *The Lancet*, vol. 394, no. 10207, pp. 1467–1480, 2024.

[2] M. B. Wallace, P. Sharma, P. Bhandari, J. East, G. Antonelli, R. Lorenzetti, M. Vieth, I. Speranza, M. Spadaccini, M. Desai *et al.*, "Impact of artificial intelligence on miss rate of colorectal neoplasia," *Gastro*, vol. 163, no. 1, pp. 295–304, 2022.

[3] J. Deng, W. Dong, R. Socher, L.-J. Li, K. Li, and L. Fei-Fei, "Imagenet: A large-scale hierarchical image database," in *IEEE CVPR*, 2009.

[4] J. Achiam, S. Adler, S. Agarwal, L. Ahmad, I. Akkaya, F. L. Aleman, D. Almeida, J. Altenschmidt, S. Altman, S. Anadkat *et al.*, "Gpt-4 technical report," *arXiv preprint arXiv:2303.08774*, 2023.

[5] X. Zhai, B. Mustafa, A. Kolesnikov, and L. Beyer, "Sigmoid loss for language image pre-training," in *IEEE ICCV*, 2023.

[6] Y. Li, S. Bubeck, R. Eldan, A. Del Giorno, S. Gunasekar, and Y. T. Lee, "Textbooks are all you need ii: phi-1.5 technical report," *arXiv preprint arXiv:2309.05463*, 2023.

[7] J. Chen, D. Zhu, X. Shen, X. Li, Z. Liu, P. Zhang, R. Krishnamoorthi, V. Chandra, Y. Xiong, and M. Elhoseiny, "Minigpt-v2: large language model as a unified interface for vision-language multitask learning," *arXiv preprint arXiv:2310.09478*, 2023.

[8] H. Liu, C. Li, Y. Li, and Y. J. Lee, "Improved baselines with visual instruction tuning," in *IEEE CVPR*, 2024.

[9] M. He, Y. Liu, B. Wu, J. Yuan, Y. Wang, T. Huang, and B. Zhao, "Efficient multimodal learning from data-centric perspective," *arXiv preprint arXiv:2402.11530*, 2024.

[10] V. S. Prasath, "Polyp detection and segmentation from video capsule endoscopy: A review," *J. Imaging*, vol. 3, no. 1, p. 1, 2016.

[11] B. Taha, N. Werghi, and J. Dias, "Automatic polyp detection in endoscopy videos: A survey," in *IEEE IASTED*, 2017.

[12] L. F. Sanchez-Peralta, L. Bote-Curiel, A. Picon, F. M. Sanchez-Margallo, and J. B. Pagador, "Deep learning to find colorectal polyps in colonoscopy: A systematic literature review," *AIIM*, vol. 108, p. 101923, 2020.

[13] I. Pacal, D. Karaboga, A. Basturk, B. Akay, and U. Nalbantoglu, "A comprehensive review of deep learning in colon cancer," *CIBM*, vol. 126, p. 104003, 2020.

[14] B. Münzer, K. Schoeffmann, and L. Böszörmenyi, "Content-based processing and analysis of endoscopic images and videos: A survey," *MTAP*, vol. 77, pp. 1323–1362, 2018.

[15] M. Taghiakbari, Y. Mori, and D. von Renteln, "Artificial intelligence-assisted colonoscopy: A review of current state of practice and research," *WJG*, vol. 27, no. 47, p. 8103, 2021.

[16] G. Yue, G. Zhuo, S. Li, T. Zhou, J. Du, W. Yan, J. Hou, W. Liu, and T. Wang, "Benchmarking polyp segmentation methods in narrow-band imaging colonoscopy images," *IEEE JBHI*, vol. 27, no. 7, pp. 3360–3371, 2023.

[17] Z. Wu, F. Lv, C. Chen, A. Hao, and S. Li, "Colorectal polyp segmentation in the deep learning era: A comprehensive survey," *arXiv preprint arXiv:2401.11734*, 2024.

[18] J. Mei, T. Zhou, K. Huang, Y. Zhang, Y. Zhou, Y. Wu, and H. Fu, "A survey on deep learning for polyp segmentation: Techniques, challenges and future trends," *arXiv preprint arXiv:2311.18373*, 2023.

[19] J. Bernal, J. Sánchez, and F. Vilarino, "Towards automatic polyp detection with a polyp appearance model," *PR*, vol. 45, no. 9, pp. 3166–3182, 2012.

[20] J. Silva, A. Histace, O. Romain, X. Dray, and B. Granado, "Toward embedded detection of polyps in wce images for early diagnosis of colorectal cancer," *CARS*, vol. 9, no. 2, pp. 283–293, 2014.

[21] J. Bernal, F. J. Sánchez, G. Fernández-Esparrach, D. Gil, C. Rodríguez, and F. Vilariño, "Wm-dova maps for accurate polyp highlighting in colonoscopy: Validation vs. saliency maps from physicians," *CMIG*, vol. 43, pp. 99–111, 2015.

[22] N. Tajbakhsh, S. R. Gurudu, and J. Liang, "Automated polyp detection in colonoscopy videos using shape and context information," *IEEE TMI*, vol. 35, no. 2, pp. 630–644, 2015.

[23] M. Ye, S. Giannarou, A. Meining, and G.-Z. Yang, "Online tracking and retargeting with applications to optical biopsy in gastrointestinal endoscopic examinations," *MedIA*, vol. 30, pp. 144–157, 2016.

[24] F. Deeba, F. M. Bui, and K. A. Wahid, "Automated growcut for segmentation of endoscopic images," in *IJCNN*, 2016.

[25] R. Zhang, Y. Zheng, T. W. C. Mak, R. Yu, S. H. Wong, J. Y. Lau, and C. C. Poon, "Automatic detection and classification of colorectal polyps by transferring low-level cnn features from nonmedical domain," *IEEE JBHI*, vol. 21, no. 1, pp. 41–47, 2016.

[26] P. Mesejo, D. Pizarro, A. Abergel, O. Rouquette, S. Beorchia, L. Poincloux, and A. Bartoli, "Computer-aided classification of gastrointestinal lesions in regular colonoscopy," *IEEE TMI*, vol. 35, no. 9, pp. 2051–2063, 2016.

[27] Q. Angermann, J. Bernal, C. Sánchez-Montes, M. Hammami, G. Fernández-Esparrach, X. Dray, O. Romain, F. J. Sánchez, and A. Histace, "Towards real-time polyp detection in colonoscopy videos: Adapting still frame-based methodologies for video sequences analysis," in *MICCAI-W*, 2017.

[28] K. Pogorelov, K. R. Randel, C. Griwodz, S. L. Eskeland, T. de Lange, D. Johansen, C. Spampinato, D.-T. Dang-Nguyen, M. Lux, P. T. Schmidt *et al.*, "Kvasir: A multi-class image dataset for computer aided gastrointestinal disease detection," in *ACM MMSys*, 2017.

[29] K. Pogorelov, K. R. Randel, T. de Lange, S. L. Eskeland, C. Griwodz, D. Johansen, C. Spampinato, M. Taschwer, M. Lux, P. T. Schmidt *et al.*, "Nerthus: A bowel preparation quality video dataset," in *ACM MMSys*, 2017.

[30] D. Vázquez, J. Bernal, F. J. Sánchez, G. Fernández-Esparrach, A. M. López, A. Romero, M. Drozdzal, and A. Courville, "A benchmark for endoluminal scene segmentation of colonoscopy images," *JHE*, vol. 2017, no. 1, p. 4037190, 2017.

[31] A. Koulaouzidis, D. K. Iakovidis, D. E. Yung, E. Rondonotti, U. Kopylov, J. N. Plevris, E. Toth, A. Eliakim, G. W. Johansson, W. Marlicz *et al.*, "Kid project: an internet-based digital video atlas of capsule endoscopy for research purposes," *EIO*, vol. 5, no. 06, pp. E477–E483, 2017.

[32] I. N. Figueiredo, L. Pinto, P. N. Figueiredo, and R. Tsai, "Unsupervised segmentation of colonic polyps in narrow-band imaging data based on manifold representation of images and wasserstein distance," *BSPC*, vol. 53, p. 101577, 2019.

[33] P. N. Figueiredo, I. N. Figueiredo, L. Pinto, S. Kumar, Y.-H. R. Tsai, and A. V. Mamonov, "Polyp detection with computer-aided diagnosis in white light colonoscopy: comparison of three different methods," *EIO*, vol. 7, no. 02, pp. E209–E215, 2019.

[34] T.-H. Hoang, H.-D. Nguyen, V.-A. Nguyen, T.-A. Nguyen, V.-T. Nguyen, and M.-T. Tran, "Enhancing endoscopic image classification with symptom localization and data augmentation," in *ACM MM*, 2019.

[35] M. Cho, J. H. Kim, K. S. Hong, J. S. Kim, H.-J. Kong, and S. Kim, "Identification of cecum time-location in a colonoscopy video by deep learning analysis of colonoscope movement," *PeerJ*, vol. 7, p. e7256, 2019.

[36] S. Ali, F. Zhou, C. Daul, B. Braden, A. Bailey, S. Realdon, J. East, G. Wagnieres, V. Loschenov, E. Grisan *et al.*, "Endoscopy artifact detection (ead 2019) challenge dataset," *arXiv preprint arXiv:1905.03209*, 2019.

[37] Y. Liu, Y. Tian, G. Maicas, L. Z. C. T. Pu, R. Singh, J. W. Verjans, and G. Carneiro, "Photoshopping colonoscopy video frames," in *IEEE ISBI*, 2020.

[38] D. Jha, P. H. Smedsrud, M. A. Riegler, P. Halvorsen, T. d. Lange, D. Johansen, and H. D. Johansen, "Kvasir-seg: A segmented polyp dataset," in *MMM*, 2020.

[39] L. F. Sánchez-Peralta, J. B. Pagador, A. Picón, Á. J. Calderón, F. Polo, N. Andraka, R. Bilbao, B. Glover, C. L. Saratxaga, and F. M. Sánchez-Margallo, "Piccolo white-light and narrow-band imaging colonoscopic dataset: a performance comparative of models and datasets," *ApplSci*, vol. 10, no. 23, p. 8501, 2020.

[40] S. Ali, N. Ghatwary, B. Braden, D. Lamarque, A. Bailey, S. Realdon, R. Cannizzaro, J. Rittscher, C. Daul, and J. East, "Endoscopy disease detection challenge 2020," *arXiv preprint arXiv:2003.03376*, 2020.

[41] R. Leenhardt, C. Li, J.-P. Le Mouel, G. Rahmi, J. C. Saurin, F. Cholet, A. Boureille, X. Amiot, M. Delvaux, C. Duburque *et al.*, "Cad-cap: a 25,000-image database serving the development of artificial intelligence for capsule endoscopy," *EIO*, vol. 8, no. 03, pp. E415–E420, 2020.

[42] C. C. Poon, Y. Jiang, R. Zhang, W. W. Lo, M. S. Cheung, R. Yu, Y. Zheng, J. C. Wong, Q. Liu, S. H. Wong *et al.*, "Ai-doscopist: a real-time deep-learning-based algorithm for localising polyps in colonoscopy videos with edge computing devices," *NPJDM*, vol. 3, no. 1, p. 73, 2020.

[43] H. Borgli, V. Thambawita, P. H. Smedsrud, S. Hicks, D. Jha, S. L. Eskeland, K. R. Randel, K. Pogorelov, M. Lux, D. T. D. Nguyen *et al.*, "Hyperkvasir, a comprehensive multi-class image and video dataset for gastrointestinal endoscopy," *SData*, vol. 7, no. 1, p. 283, 2020.

[44] X. Guo, C. Yang, Y. Liu, and Y. Yuan, "Learn to threshold: Thresholdnet with confidence-guided manifold mixup for polyp segmentation," *IEEE TMI*, vol. 40, no. 4, pp. 1134–1146, 2020.

[45] S. Ali, M. Dmitrieva, N. Ghatwary, S. Bano, G. Polat, A. Temizel, A. Krenzer, A. Hekalo, Y. B. Guo, B. Matuszewski *et al.*, "Deep learning for detection and segmentation of artefact and disease instances in gastrointestinal endoscopy," *MedIA*, vol. 70, p. 102002, 2021.

[46] P. Ngoc Lan, N. S. An, D. V. Hang, D. V. Long, T. Q. Trung, N. T. Thuy, and D. V. Sang, "Neounet: Towards accurate colon polyp segmentation and neoplasm detection," in *ISVC*, 2021.

[47] Q. Wang, H. Che, W. Ding, L. Xiang, G. Li, Z. Li, and S. Cui, "Colorectal polyp classification from white-light colonoscopy images via domain alignment," in *MICCAI*, 2021.

[48] Y. Ma, X. Chen, K. Cheng, Y. Li, and B. Sun, "Ldpolypvideo benchmark: a large-scale colonoscopy video dataset of diverse polyps," in *MICCAI*, 2021.

[49] N. Celik, S. Ali, S. Gupta, B. Braden, and J. Rittscher, "Endouda: a modality independent segmentation approach for endoscopy imaging," in *MICCAI*, 2021.

[50] D. Jha, S. Ali, K. Emanuelsen, S. A. Hicks, V. Thambawita, E. Garcia-Ceja, M. A. Riegler, T. de Lange, P. T. Schmidt, H. D. Johansen *et al.*, "Kvasir-instrument: Diagnostic and therapeutic tool segmentation dataset in gastrointestinal endoscopy," in *MMM*, 2021.

[51] W. Wang, J. Tian, C. Zhang, Y. Luo, X. Wang, and J. Li, "An improved deep learning approach and its applications on colonic polyp images detection," *BMCMI*, vol. 20, pp. 1–14, 2020.

[52] A. de Maissin, R. Vallée, M. Flamant, M. Fondain-Bossiere, C. Le Berre, A. Coutrot, N. Normand, H. Mouchère, S. Coudol, C. Trang *et al.*, "Multi-expert annotation of crohn's disease images of the small bowel for automatic detection using a convolutional recurrent attention neural network," *EIO*, vol. 9, no. 07, pp. E1136–E1144, 2021.

[53] Z. Kong, M. He, Q. Luo, X. Huang, P. Wei, Y. Cheng, L. Chen, Y. Liang, Y. Lu, X. Li *et al.*, "Multi-task classification and segmentation for explicable capsule endoscopy diagnostics," *FMOLB*, vol. 8, p. 614277, 2021.

[54] M. Misawa, S.-e. Kudo, Y. Mori, K. Hotta, K. Ohtsuka, T. Matsuda, S. Saito, T. Kudo, T. Baba, F. Ishida *et al.*, "Development of a computer-aided detection system for colonoscopy and a publicly accessible large colonoscopy video database (with video)," *GIE*, vol. 93, no. 4, pp. 960–967, 2021.

[55] D. Jha, P. H. Smedsrud, D. Johansen, T. de Lange, H. D. Johansen, P. Halvorsen, and M. A. Riegler, "A comprehensive study on colorectal polyp segmentation with resunet++, conditional random field and test-time augmentation," *IEEE JBHI*, vol. 25, no. 6, pp. 2029–2040, 2021.

[56] P. H. Smedsrud, V. Thambawita, S. A. Hicks, H. Gjestang, O. O. Nedrejord, E. Næss, H. Borgli, D. Jha, T. J. D. Berstad, S. L. Eskeland *et al.*, "Kvasir-capsule, a video capsule endoscopy dataset," *SData*, vol. 8, no. 1, p. 142, 2021.

[57] K. Li, M. I. Fathan, K. Patel, T. Zhang, C. Zhong, A. Bansal, A. Rastogi, J. S. Wang, and G. Wang, "Colonoscopy polyp detection and classification: Dataset creation and comparative evaluations," *PONE*, vol. 16, no. 8, p. e0255809, 2021.

[58] J. Cychnerski, T. Dziubich, and A. Brzeski, "Ers: a novel comprehensive endoscopy image dataset for machine learning, compliant with the mst 3.0 specification," *arXiv preprint arXiv:2201.08746*, 2022.

[59] Y. Tian, G. Pang, F. Liu, Y. Liu, C. Wang, Y. Chen, J. Verjans, and G. Carneiro, "Contrastive transformer-based multiple instance learning for weakly supervised polyp frame detection," in *MICCAI*, 2022.

[60] F. J. P. Montalbo, "Diagnosing gastrointestinal diseases from endoscopy images through a multi-fused cnn with auxiliary layers, alpha dropouts, and a fusion residual block," *BSPC*, vol. 76, p. 103683, 2022.

[61] S. Ali and N. Ghatwary, "Endoscopic computer vision challenges 2.0," 2022. [Online]. Available: https://endocv2022.grand-challenge.org/

[62] G.-P. Ji, G. Xiao, Y.-C. Chou, D.-P. Fan, K. Zhao, G. Chen, and L. Van Gool, "Video polyp segmentation: A deep learning perspective," *MIR*, vol. 19, no. 6, pp. 531–549, 2022.

[63] V. Thambawita, P. Salehi, S. A. Sheshkal, S. A. Hicks, H. L. Hammer, S. Parasa, T. d. Lange, P. Halvorsen, and M. A. Riegler, "Singan-seg: Synthetic training data generation for medical image segmentation," *PONE*, vol. 17, no. 5, p. e0267976, 2022.

[64] D. Fitting, A. Krenzer, J. Troya, M. Banck, B. Sudarevic, M. Brand, W. Böck, W. G. Zoller, T. Rösch, F. Puppe *et al.*, "A video based benchmark data set (endotest) to evaluate computer-aided polyp detection systems," *SJG*, vol. 57, no. 11, pp. 1397–1403, 2022.

[65] S. Hicks, A. Storås, P. Halvorsen, T. de Lange, M. Riegler, and V. Thambawita, "Overview of imageclef medical 2023–medical visual question answering for gastrointestinal tract," in *CLEF (Working notes)*, 2023.

[66] D. Jha, V. Sharma, N. Dasu, N. K. Tomar, S. Hicks, M. Bhuyan, P. K. Das, M. A. Riegler, P. Halvorsen, T. de Lange *et al.*, "Gastrovision: A multi-class endoscopy image dataset for computer aided gastrointestinal disease detection," in *ICML-W*, 2023.

[67] G. Ren, M. Lazarou, J. Yuan, and T. Stathaki, "Towards automated polyp segmentation using weakly-and semi-supervised learning and deformable transformers," in *IEEE CVPR-W*, 2023.

[68] G. Polat, H. T. Kani, I. Ergenc, Y. Ozen Alahdab, A. Temizel, and O. Atug, "Improving the computer-aided estimation of ulcerative colitis severity according to mayo endoscopic score by using regression-based deep learning," *IBD*, vol. 29, no. 9, pp. 1431–1439, 2023.

[69] S. Ali, D. Jha, N. Ghatwary, S. Realdon, R. Cannizzaro, O. E. Salem, D. Lamarque, C. Daul, M. A. Riegler, K. V. Anonsen *et al.*, "A multi-centre polyp detection and segmentation dataset for generalisability assessment," *SData*, vol. 10, no. 1, p. 75, 2023.

[70] D. Wang, X. Wang, L. Wang, M. Li, Q. Da, X. Liu, X. Gao, J. Shen, J. He, T. Shen *et al.*, "A real-world dataset and benchmark for foundation model adaptation in medical image classification," *SData*, vol. 10, no. 1, p. 574, 2023.

[71] H. Khan, Ali; Malik, "Gastrointestinal bleeding wce images dataset," 2023, doi: 10.17632/8pbbjf274w.1.

[72] C. Biffi, G. Antonelli, S. Bernhofer, C. Hassan, D. Hirata, M. Iwatate, A. Maieron, P. Salvagnini, and A. Cherubini, "Realcolon: A dataset for developing real-world ai applications in colonoscopy," *SData*, vol. 11, no. 1, p. 539, 2024.

[73] Z. Xu, J. Rittscher, and S. Ali, "Ssl-cpcd: Self-supervised learning with composite pretext-class discrimination for improved generalisability in endoscopic image analysis," *IEEE TMI*, 2024, doi: 10.1109/TMI.2024.3411933.

[74] S. Gautam, A. Storås, C. Midoglu, S. A. Hicks, V. Thambawita, P. Halvorsen, and M. A. Riegler, "Kvasir-vqa: A text-image pair gi tract dataset," in *ACM MM-W*, 2024.

[75] P. Handa, A. Mahbod, F. Schwarzhans, R. Woitek, N. Goel, D. Chhabra, S. Jha, M. Dhir, D. Gunjan, J. Kakarla *et al.*, "Capsule vision 2024 challenge: Multi-class abnormality classification for video capsule endoscopy," in *CVIP*, 2024.

[76] L. Ruiz, F. Sierra-Jerez, J. Ruiz, and F. Martinez, "Colon: The largest colonoscopy long sequence public database," *arXiv preprint arXiv:2403.00663*, 2024.

[77] P. Handa, M. Dhir, A. Mahbod, F. Schwarzhans, R. Woitek, N. Goel, and D. Gunjan, "Wcebleedgen: A wireless capsule endoscopy dataset and its benchmarking for automatic bleeding classification, detection, and segmentation," *arXiv preprint arXiv:2408.12466*, 2024.

[78] D. Jha, N. K. Tomar, V. Sharma, Q.-H. Trinh, K. Biswas, H. Pan, R. K. Jha, G. Durak, A. Hann, J. Varkey *et al.*, "Polypdb: A

[79] curated multi-center dataset for development of ai algorithms in colonoscopy," *arXiv preprint arXiv:2409.00045*, 2024.

[79] M. Sivak, "Gastrointestinal endoscopy: past and future," *Gut*, vol. 55, no. 8, pp. 1061–1064, 2006.

[80] T. M. Berzin and E. J. Topol, "Adding artificial intelligence to gastrointestinal endoscopy," *The Lancet*, vol. 395, no. 10223, p. 485, 2020.

[81] G. Iddan, G. Meron, A. Glukhovsky, and P. Swain, "Wireless capsule endoscopy," *Nature*, vol. 405, no. 6785, pp. 417–417, 2000.

[82] R. Anteby, N. Horesh, S. Soffer, Y. Zager, Y. Barash, I. Amiel, D. Rosin, M. Gutman, and E. Klang, "Deep learning visual analysis in laparoscopic surgery: a systematic review and diagnostic test accuracy meta-analysis," *SEND*, vol. 35, pp. 1521–1533, 2021.

[83] S. Shao, Z. Pei, W. Chen, W. Zhu, X. Wu, D. Sun, and B. Zhang, "Self-supervised monocular depth and ego-motion estimation in endoscopy: Appearance flow to the rescue," *MedIA*, vol. 77, p. 102338, 2022.

[84] J. C. Á. Cerón, G. O. Ruiz, L. Chang, and S. Ali, "Real-time instance segmentation of surgical instruments using attention and multi-scale feature fusion," *MedIA*, vol. 81, p. 102569, 2022.

[85] Y. Blau, D. Freedman, V. Dashinsky, R. Goldenberg, and E. Rivlin, "Unsupervised 3d shape coverage estimation with applications to colonoscopy," in *IEEE ICCV-W*, 2021.

[86] Y. Zhang, S. Wang, R. Ma, S. K. McGill, J. G. Rosenman, and S. M. Pizer, "Lighting enhancement aids reconstruction of colonoscopic surfaces," in *IPMI*, 2021.

[87] D.-P. Fan, G.-P. Ji, P. Xu, M.-M. Cheng, C. Sakaridis, and L. Van Gool, "Advances in deep concealed scene understanding," *VI*, vol. 1, no. 1, p. 16, 2023.

[88] W. M. de Vos and E. A. de Vos, "Role of the intestinal microbiome in health and disease: from correlation to causation," *Nutr. Rev.*, vol. 70, no. suppl_1, pp. S45–S56, 2012.

[89] Y. Li and P. Agarwal, "A pathway-based view of human diseases and diseases relationships," *PONE*, vol. 4, no. 2, p. e4346, 2009.

[90] B. Veauthier and J. R. Hornecker, "Crohn's disease: diagnosis and management," *AFP*, vol. 98, no. 11, pp. 661–669, 2018.

[91] L. Yang, H. Jiang, Q. Song, and J. Guo, "A survey on long-tailed visual recognition," *IJCV*, vol. 130, no. 7, pp. 1837–1872, 2022.

[92] J. Wu, X. Li, S. X. H. Yuan, H. Ding, Y. Yang, X. Li, J. Zhang, Y. Tong, X. Jiang, B. Ghanem *et al.*, "Towards open vocabulary learning: A survey," *IEEE TPAMI*, vol. 46, no. 7, pp. 5092–5113, 2024.

[93] K. Singhal, S. Azizi, T. Tu, S. S. Mahdavi, J. Wei, H. W. Chung, N. Scales, A. Tanwani, H. Cole-Lewis, S. Pfohl *et al.*, "Large language models encode clinical knowledge," *Nature*, vol. 620, no. 7972, pp. 172–180, 2023.

[94] J. Zhang, Y. Xie, Y. Xia, and C. Shen, "Dodnet: Learning to segment multi-organ and tumors from multiple partially labeled datasets," in *IEEE CVPR*, 2021.

[95] D. Karimi, H. Dou, S. K. Warfield, and A. Gholipour, "Deep learning with noisy labels: Exploring techniques and remedies in medical image analysis," *MedIA*, vol. 65, p. 101759, 2020.

[96] H.-F. Yu, P. Jain, P. Kar, and I. Dhillon, "Large-scale multi-label learning with missing labels," in *ICML*, 2014.

[97] Y. Jia, E. Shelhamer, J. Donahue, S. Karayev, J. Long, R. Girshick, S. Guadarrama, and T. Darrell, "Caffe: Convolutional architecture for fast feature embedding," in *ACM MM*, 2014.

[98] G. Huang, Z. Liu, L. Van Der Maaten, and K. Q. Weinberger, "Densely connected convolutional networks," in *IEEE CVPR*, 2017.

[99] K. He, X. Zhang, S. Ren, and J. Sun, "Deep residual learning for image recognition," in *IEEE CVPR*, 2016.

[100] A. Dosovitskiy, L. Beyer, A. Kolesnikov, D. Weissenborn, X. Zhai, T. Unterthiner, M. Dehghani, M. Minderer, G. Heigold, S. Gelly *et al.*, "An image is worth 16x16 words: Transformers for image recognition at scale," in *ICLR*, 2021.

[101] M. Sandler, A. Howard, M. Zhu, A. Zhmoginov, and L.-C. Chen, "Mobilenetv2: Inverted residuals and linear bottlenecks," in *IEEE CVPR*, 2018.

[102] S. Woo, J. Park, J.-Y. Lee, and I. S. Kweon, "Cbam: Convolutional block attention module," in *ECCV*, 2018.

[103] D. Tran, L. Bourdev, R. Fergus, L. Torresani, and M. Paluri, "Learning spatiotemporal features with 3d convolutional networks," in *IEEE ICCV*, 2015.

[104] C. Szegedy, V. Vanhoucke, S. Ioffe, J. Shlens, and Z. Wojna, "Rethinking the inception architecture for computer vision," in *IEEE CVPR*, 2016.

[105] J. Carreira and A. Zisserman, "Quo vadis, action recognition? a new model and the kinetics dataset," in *IEEE CVPR*, 2017.

[106] Y. Yuan, W. Qin, B. Ibragimov, B. Han, and L. Xing, "Riis-densenet: rotation-invariant and image similarity constrained densely connected convolutional network for polyp detection," in *MICCAI*, 2018.

[107] Y. Tian, G. Maicas, L. Z. C. T. Pu, R. Singh, J. W. Verjans, and G. Carneiro, "Few-shot anomaly detection for polyp frames from colonoscopy," in *MICCAI*, 2020.

[108] H. Gammulle, S. Denman, S. Sridharan, and C. Fookes, "Two-stream deep feature modelling for automated video endoscopy data analysis," in *MICCAI*, 2020.

[109] G. Carneiro, L. Z. C. T. Pu, R. Singh, and A. Burt, "Deep learning uncertainty and confidence calibration for the five-class polyp classification from colonoscopy," *MedIA*, vol. 62, p. 101653, 2020.

[110] X. Guo and Y. Yuan, "Semi-supervised wce image classification with adaptive aggregated attention," *MedIA*, vol. 64, p. 101733, 2020.

[111] W. Ma, Y. Zhu, R. Zhang, J. Yang, Y. Hu, Z. Li, and L. Xiang, "Toward clinically assisted colorectal polyp recognition via structured cross-modal representation consistency," in *MICCAI*, 2022.

[112] K.-N. Wang, Y. He, S. Zhuang, J. Miao, X. He, P. Zhou, G. Yang, G.-Q. Zhou, and S. Li, "Ffcnet: Fourier transform-based frequency learning and complex convolutional network for colon disease classification," in *MICCAI*, 2022.

[113] K.-N. Wang, S. Zhuang, Q.-Y. Ran, P. Zhou, J. Hua, G.-Q. Zhou, and X. He, "Dlgnet: A dual-branch lesion-aware network with the supervised gaussian mixture model for colon lesions classification in colonoscopy images," *MedIA*, vol. 87, p. 102832, 2023.

[114] G. Yue, P. Wei, Y. Liu, Y. Luo, J. Du, and T. Wang, "Automated endoscopic image classification via deep neural network with class imbalance loss," *IEEE TIM*, vol. 72, pp. 1–11, 2023.

[115] Y. Luo, X. Guo, L. Liu, and Y. Yuan, "Dynamic attribute-guided few-shot open-set network for medical image diagnosis," *ESWA*, vol. 251, p. 124098, 2024.

[116] H. Itoh, H. R. Roth, L. Lu, M. Oda, M. Misawa, Y. Mori, S.-e. Kudo, and K. Mori, "Towards automated colonoscopy diagnosis: binary polyp size estimation via unsupervised depth learning," in *MICCAI*, 2018.

[117] J. Schmidhuber, S. Hochreiter *et al.*, "Long short-term memory," *Neural Comput.*, vol. 9, no. 8, pp. 1735–1780, 1997.

[118] M. F. Byrne, N. Chapados, F. Soudan, C. Oertel, M. L. Pérez, R. Kelly, N. Iqbal, F. Chandelier, and D. K. Rex, "Real-time differentiation of adenomatous and hyperplastic diminutive colorectal polyps during analysis of unaltered videos of standard colonoscopy using a deep learning model," *Gut*, vol. 68, no. 1, pp. 94–100, 2019.

[119] A. Tamhane, T. Mida, E. Posner, and M. Bouhnik, "Colonoscopy landmark detection using vision transformers," in *MICCAI-W*, 2022.

[120] A. Bochkovskiy, C.-Y. Wang, and H.-Y. M. Liao, "Yolov4: Optimal speed and accuracy of object detection," *arXiv preprint arXiv:2004.10934*, 2020.

[121] J. Redmon, "Yolov3: An incremental improvement," *arXiv preprint arXiv:1804.02767*, 2018.

[122] M. Tan, R. Pang, and Q. V. Le, "Efficientdet: Scalable and efficient object detection," in *IEEE CVPR*, 2020.

[123] B. Li, W. Wu, Q. Wang, F. Zhang, J. Xing, and J. Yan, "Siamrpn++: Evolution of siamese visual tracking with very deep networks," in *IEEE CVPR*, 2019.

[124] K. Simonyan and A. Zisserman, "Very deep convolutional networks for large-scale image recognition," in *ICLR*, 2015.

[125] K. He, X. Zhang, S. Ren, and J. Sun, "Identity mappings in deep residual networks," in *ECCV*, 2016.

[126] X. Yang, Q. Wei, C. Zhang, K. Zhou, L. Kong, and W. Jiang, "Colon polyp detection and segmentation based on improved mrcnn," *IEEE TIM*, vol. 70, pp. 1–10, 2020.

[127] X. Liu, X. Guo, Y. Liu, and Y. Yuan, "Consolidated domain adaptive detection and localization framework for cross-device colonoscopic images," *MedIA*, vol. 71, p. 102052, 2021.

[128] H. A. Qadir, Y. Shin, J. Solhusvik, J. Bergsland, L. Aabakken, and I. Balasingham, "Toward real-time polyp detection using fully cnns for 2d gaussian shapes prediction," *MedIA*, vol. 68, p. 101897, 2021.

[129] X. Liu, W. Li, and Y. Yuan, "Intervention & interaction federated abnormality detection with noisy clients," in *MICCAI*, 2022.

[130] I. Pacal, A. Karaman, D. Karaboga, B. Akay, A. Basturk, U. Nalbantoglu, and S. Coskun, "An efficient real-time colonic polyp detection with yolo algorithms trained by using negative samples and large datasets," *CIBM*, vol. 141, p. 105031, 2022.

[131] X. Liu and Y. Yuan, "A source-free domain adaptive polyp detection framework with style diversification flow," *IEEE TMI*, vol. 41, no. 7, pp. 1897–1908, 2022.

[132] R. Gong, S. He, T. Tian, J. Chen, Y. Hao, and C. Qiao, "Frcnn-aa-cif: An automatic detection model of colon polyps based on attention awareness and context information fusion," *CIBM*, vol. 158, p. 106787, 2023.

[133] M. R. Haugland, H. A. Qadir, and I. Balasingham, "Deep learning for improved polyp detection from synthetic narrow-band imaging," in *SPIE Med. Imaging*, 2023.

[134] W. Li, X. Liu, and Y. Yuan, "Scan++: Enhanced semantic conditioned adaptation for domain adaptive object detection," *IEEE TMM*, vol. 25, pp. 7051–7061, 2023.

[135] X. Pan, Y. Mu, C. Ma, and Q. He, "Tfcnet: A texture-aware and fine-grained feature compensated polyp detection network," *CIBM*, vol. 171, p. 108144, 2024.

[136] X. Liu, W. Li, and Y. Yuan, "Decoupled unbiased teacher for source-free domain adaptive medical object detection," *IEEE TNNLS*, vol. 35, no. 6, pp. 7287–7298, 2024.

[137] Tajbakhsh, Nima and Gurudu, Suryakanth R and Liang, Jianming, "A comprehensive computer-aided polyp detection system for colonoscopy videos," in *IPMI*, 2015.

[138] L. Yu, H. Chen, Q. Dou, J. Qin, and P. A. Heng, "Integrating online and offline three-dimensional deep learning for automated polyp detection in colonoscopy videos," *IEEE JBHI*, vol. 21, no. 1, pp. 65–75, 2016.

[139] X. Mo, K. Tao, Q. Wang, and G. Wang, "An efficient approach for polyps detection in endoscopic videos based on faster r-cnn," in *IEEE ICPR*, 2018.

[140] S. Ren, K. He, R. Girshick, and J. Sun, "Faster r-cnn: Towards real-time object detection with region proposal networks," in *NeurIPS*, 2015.

[141] H. A. Qadir, I. Balasingham, J. Solhusvik, J. Bergsland, L. Aabakken, and Y. Shin, "Improving automatic polyp detection using cnn by exploiting temporal dependency in colonoscopy video," *IEEE JBHI*, vol. 24, no. 1, pp. 180–193, 2019.

[142] Z. Zhang, H. Shang, H. Zheng, X. Wang, J. Wang, Z. Sun, J. Huang, and J. Yao, "Asynchronous in parallel detection and tracking (aipdt): Real-time robust polyp detection," in *MICCAI*, 2020.

[143] L. Wu, Z. Hu, Y. Ji, P. Luo, and S. Zhang, "Multi-frame collaboration for effective endoscopic video polyp detection via spatial-temporal feature transformation," in *MICCAI*, 2021.

[144] T. Yu, N. Lin, X. Zhang, Y. Pan, H. Hu, W. Zheng, J. Liu, W. Hu, H. Duan, and J. Si, "An end-to-end tracking method for polyp detectors in colonoscopy videos," *AIIM*, vol. 131, p. 102363, 2022.

[145] D. Wang, X. Wang, S. Wang, and Y. Yin, "Explainable multitask shapley explanation networks for real-time polyp diagnosis in videos," *IEEE TII*, vol. 19, no. 6, pp. 7780–7789, 2022.

[146] Y. Jiang, Z. Zhang, R. Zhang, G. Li, S. Cui, and Z. Li, "Yona: You only need one adjacent reference-frame for accurate and fast video polyp detection," in *MICCAI*, 2023.

[147] Y. Intrator, N. Aizenberg, A. Livne, E. Rivlin, and R. Goldenberg, "Self-supervised polyp re-identification in colonoscopy," in *MICCAI*, 2023.

[148] Y. Jiang, Z. Zhang, J. Wei, C.-M. Feng, G. Li, X. Wan, S. Cui, and Z. Li, "Let video teaches you more: Video-to-image knowledge distillation using detection transformer for medical video lesion detection," *arXiv preprint arXiv:2408.14051*, 2024.

[149] L. Zhu, B. Liao, Q. Zhang, X. Wang, W. Liu, and X. Wang, "Vision mamba: Efficient visual representation learning with bidirectional state space model," in *ICML*, 2024.

[150] A. Radford, J. W. Kim, C. Hallacy, A. Ramesh, G. Goh, S. Agarwal, G. Sastry, A. Askell, P. Mishkin, J. Clark *et al.*, "Learning transferable visual models from natural language supervision," in *ICML*, 2021.

[151] W. Liu, D. Anguelov, D. Erhan, C. Szegedy, S. Reed, C.-Y. Fu, and A. C. Berg, "Ssd: Single shot multibox detector," in *ECCV*, 2016.

[152] J. Bernal, N. Tajkbaksh, F. J. Sanchez, B. J. Matuszewski, H. Chen, L. Yu, Q. Angermann, O. Romain, B. Rustad, I. Balasingham *et al.*, "Comparative validation of polyp detection methods in video colonoscopy: results from the miccai 2015 endoscopic vision challenge," *IEEE TMI*, vol. 36, no. 6, pp. 1231–1249, 2017.

[153] Z. Zhang, Q. Liu, and Y. Wang, "Road extraction by deep residual u-net," *IEEE GRSL*, vol. 15, no. 5, pp. 749–753, 2018.

[154] S.-H. Gao, M.-M. Cheng, K. Zhao, X.-Y. Zhang, M.-H. Yang, and P. Torr, "Res2net: A new multi-scale backbone architecture," *IEEE TPAMI*, vol. 43, no. 2, pp. 652–662, 2019.

[155] H. Touvron, M. Cord, M. Douze, F. Massa, A. Sablayrolles, and H. Jégou, "Training data-efficient image transformers & distillation through attention," in *ICML*, 2021.

[156] M. Tan and Q. Le, "Efficientnet: Rethinking model scaling for convolutional neural networks," in *ICML*, 2019.

[157] L.-C. Chen, Y. Zhu, G. Papandreou, F. Schroff, and H. Adam, "Encoder-decoder with atrous separable convolution for semantic image segmentation," in *ECCV*, 2018.

[158] W. Wang, E. Xie, X. Li, D.-P. Fan, K. Song, D. Liang, T. Lu, P. Luo, and L. Shao, "Pvt v2: Improved baselines with pyramid vision transformer," *CVMJ*, vol. 8, no. 3, pp. 415–424, 2022.

[159] H. Wu, B. Xiao, N. Codella, M. Liu, X. Dai, L. Yuan, and L. Zhang, "Cvt: Introducing convolutions to vision transformers," in *IEEE ICCV*, 2021.

[160] E. Xie, W. Wang, Z. Yu, A. Anandkumar, J. M. Alvarez, and P. Luo, "Segformer: Simple and efficient design for semantic segmentation with transformers," in *NeurIPS*, 2021.

[161] S. Chen, E. Xie, C. Ge, R. Chen, D. Liang, and P. Luo, "Cyclemlp: A mlp-like architecture for dense prediction," in *ICLR*, 2022.

[162] L. Chen, T. Yang, X. Zhang, W. Zhang, and J. Sun, "Points as queries: Weakly semi-supervised object detection by points," in *IEEE CVPR*, 2021.

[163] M.-H. Guo, C.-Z. Lu, Q. Hou, Z. Liu, M.-M. Cheng, and S.-M. Hu, "Segnext: Rethinking convolutional attention design for semantic segmentation," in *NeurIPS*, 2022.

[164] Z. Liu, Y. Lin, Y. Cao, H. Hu, Y. Wei, Z. Zhang, S. Lin, and B. Guo, "Swin transformer: Hierarchical vision transformer using shifted windows," in *IEEE ICCV*, 2021.

[165] A. Kirillov, E. Mintun, N. Ravi, H. Mao, C. Rolland, L. Gustafson, T. Xiao, S. Whitehead, A. C. Berg, W.-Y. Lo, P. Dollar, and R. Girshick, "Segment anything," in *IEEE ICCV*, 2023.

[166] N. Ravi, V. Gabeur, Y.-T. Hu, R. Hu, C. Ryali, T. Ma, H. Khedr, R. Rädle, C. Rolland, L. Gustafson *et al.*, "Sam 2: Segment anything in images and videos," *arXiv preprint arXiv:2408.00714*, 2024.

[167] L.-C. Chen, G. Papandreou, I. Kokkinos, K. Murphy, and A. L. Yuille, "Deeplab: Semantic image segmentation with deep convolutional nets, atrous convolution, and fully connected crfs," *IEEE TPAMI*, vol. 40, no. 4, pp. 834–848, 2017.

[168] J. Wang, K. Sun, T. Cheng, B. Jiang, C. Deng, Y. Zhao, D. Liu, Y. Mu, M. Tan, X. Wang *et al.*, "Deep high-resolution representation learning for visual recognition," *IEEE TPAMI*, vol. 43, no. 10, pp. 3349–3364, 2020.

[169] Z. Liu, H. Mao, C.-Y. Wu, C. Feichtenhofer, T. Darrell, and S. Xie, "A convnet for the 2020s," in *IEEE CVPR*, 2022.

[170] B. Cheng, I. Misra, A. G. Schwing, A. Kirillov, and R. Girdhar, "Masked-attention mask transformer for universal image segmentation," in *IEEE CVPR*, 2022, pp. 1290–1299.

[171] Y. Yuan, D. Li, and M. Q.-H. Meng, "Automatic polyp detection via a novel unified bottom-up and top-down saliency approach," *IEEE JBHI*, vol. 22, no. 4, pp. 1250–1260, 2017.

[172] Y. Fang, C. Chen, Y. Yuan, and K.-y. Tong, "Selective feature aggregation network with area-boundary constraints for polyp segmentation," in *MICCAI*, 2019.

[173] D. Jha, P. H. Smedsrud, M. A. Riegler, D. Johansen, T. De Lange, P. Halvorsen, and H. D. Johansen, "Resunet++: An advanced architecture for medical image segmentation," in *IEEE ISM*, 2019.

[174] R. Zhang, G. Li, Z. Li, S. Cui, D. Qian, and Y. Yu, "Adaptive context selection for polyp segmentation," in *MICCAI*, 2020.

[175] D.-P. Fan, G.-P. Ji, T. Zhou, G. Chen, H. Fu, J. Shen, and L. Shao, "Pranet: Parallel reverse attention network for polyp segmentation," in *MICCAI*, 2020.

[176] K. Wickstrøm, M. Kampffmeyer, and R. Jenssen, "Uncertainty and interpretability in convolutional neural networks for semantic segmentation of colorectal polyps," *MedIA*, vol. 60, p. 101619, 2020.

[177] H. Wu, J. Zhong, W. Wang, Z. Wen, and J. Qin, "Precise yet efficient semantic calibration and refinement in convnets for real-time polyp segmentation from colonoscopy videos," in *AAAI*, 2021.

[178] Y. Meng, H. Zhang, D. Gao, Y. Zhao, X. Yang, X. Qian, X. Huang, and Y. Zheng, "Bi-gcn: Boundary-aware input-dependent graph convolution network for biomedical image segmentation," in *BMVC*, 2021.

[179] H. Wu, G. Chen, Z. Wen, and J. Qin, "Collaborative and adversarial learning of focused and dispersive representations for semi-supervised polyp segmentation," in *IEEE ICCV*, 2021.

[180] T.-C. Nguyen, T.-P. Nguyen, G.-H. Diep, A.-H. Tran-Dinh, T. V. Nguyen, and M.-T. Tran, "Ccbanet: cascading context and balancing attention for polyp segmentation," in *MICCAI*, 2021.

[181] Y. Tian, G. Pang, F. Liu, Y. Chen, S. H. Shin, J. W. Verjans, R. Singh, and G. Carneiro, "Constrained contrastive distribution learning for unsupervised anomaly detection and localisation in medical images," in *MICCAI*, 2021.

[182] Y. Shen, X. Jia, and M. Q.-H. Meng, "Hrenet: A hard region enhancement network for polyp segmentation," in *MICCAI*, 2021.

[183] M. Cheng, Z. Kong, G. Song, Y. Tian, Y. Liang, and J. Chen, "Learnable oriented-derivative network for polyp segmentation," in *MICCAI*, 2021.

[184] X. Zhao, L. Zhang, and H. Lu, "Automatic polyp segmentation via multi-scale subtraction network," in *MICCAI*, 2021.

[185] J. Wei, Y. Hu, R. Zhang, Z. Li, S. K. Zhou, and S. Cui, "Shallow attention network for polyp segmentation," in *MICCAI*, 2021.

[186] Y. Zhang, H. Liu, and Q. Hu, "Transfuse: Fusing transformers and cnns for medical image segmentation," in *MICCAI*, 2021.

[187] T. Kim, H. Lee, and D. Kim, "Uacanet: Uncertainty augmented context attention for polyp segmentation," in *ACM MM*, 2021.

[188] C. Yang, X. Guo, M. Zhu, B. Ibragimov, and Y. Yuan, "Mutual-prototype adaptation for cross-domain polyp segmentation," *IEEE JBHI*, vol. 25, no. 10, pp. 3886–3897, 2021.

[189] X. Guo, C. Yang, and Y. Yuan, "Dynamic-weighting hierarchical segmentation network for medical images," *MedIA*, vol. 73, p. 102196, 2021.

[190] X. Du, X. Xu, and K. Ma, "Icgnet: Integration context-based reverse-contour guidance network for polyp segmentation," in *IJCAI*, 2022.

[191] J. Wei, Y. Hu, G. Li, S. Cui, S. Kevin Zhou, and Z. Li, "Boxpolyp: Boost generalized polyp segmentation using extra coarse bounding box annotations," in *MICCAI*, 2022.

[192] R. Zhang, P. Lai, X. Wan, D.-J. Fan, F. Gao, X.-J. Wu, and G. Li, "Lesion-aware dynamic kernel for polyp segmentation," in *MICCAI*, 2022.

[193] L. Cai, M. Wu, L. Chen, W. Bai, M. Yang, S. Lyu, and Q. Zhao, "Using guided self-attention with local information for polyp segmentation," in *MICCAI*, 2022.

[194] J. Wang, Q. Huang, F. Tang, J. Meng, J. Su, and S. Song, "Stepwise feature fusion: Local guides global," in *MICCAI*, 2022.

[195] Y. Shen, Y. Lu, X. Jia, F. Bai, and M. Q.-H. Meng, "Task-relevant feature replenishment for cross-centre polyp segmentation," in *MICCAI*, 2022.

[196] D. Wang, S. Chen, Q. Chen, Y. Cao, B. Liu, X. Liu, and X. Sun, "Afp-mask: Anchor-free polyp instance segmentation in colonoscopy," *IEEE JBHI*, vol. 26, no. 7, pp. 2995–3006, 2022.

[197] G. Yue, W. Han, B. Jiang, T. Zhou, R. Cong, and T. Wang, "Boundary constraint network with cross layer feature integration for polyp segmentation," *IEEE JBHI*, vol. 26, no. 8, pp. 4090–4099, 2022.

[198] Y. Lin, J. Wu, G. Xiao, J. Guo, G. Chen, and J. Ma, "Bsca-net: Bit slicing context attention network for polyp segmentation," *PR*, vol. 132, p. 108917, 2022.

[199] J.-H. Shi, Q. Zhang, Y.-H. Tang, and Z.-Q. Zhang, "Polyp-mixer: An efficient context-aware mlp-based paradigm for polyp segmentation," *IEEE TCSVT*, vol. 33, no. 1, pp. 30–42, 2022.

[200] H. Wu, W. Xie, J. Lin, and X. Guo, "Acl-net: semi-supervised polyp segmentation via affinity contrastive learning," in *AAAI*, 2023.

[201] J. Wei, Y. Hu, S. Cui, S. K. Zhou, and Z. Li, "Weakpolyp: You only look bounding box for polyp segmentation," in *MICCAI*, 2023.

[202] T. Ling, C. Wu, H. Yu, T. Cai, D. Wang, Y. Zhou, M. Chen, and K. Ding, "Probabilistic modeling ensemble vision transformer improves complex polyp segmentation," in *MICCAI*, 2023.

[203] A. Wang, M. Xu, Y. Zhang, M. Islam, and H. Ren, "S^{2}me: Spatial-spectral mutual teaching and ensemble learning for scribble-supervised polyp segmentation," in *MICCAI*, 2023.

[204] Y. Su, Y. Shen, J. Ye, J. He, and J. Cheng, "Revisiting feature propagation and aggregation in polyp segmentation," in *MICCAI*, 2023.

[205] B. Dong, W. Wang, D.-P. Fan, J. Li, H. Fu, and L. Shao, "Polyp-pvt: Polyp segmentation with pyramid vision transformers," *CAAI AIR*, vol. 2, p. 9150015, 2023.

[206] J. Wang and C. Chen, "Unsupervised adaptation of polyp segmentation models via coarse-to-fine self-supervision," in *IPMI*, 2023.

[207] Q. Jin, H. Hou, G. Zhang, and Z. Li, "Fegnet: A feedback enhancement gate network for automatic polyp segmentation," *IEEE JBHI*, vol. 27, no. 7, pp. 3420–3430, 2023.

[208] J. Du, K. Guan, P. Liu, Y. Li, and T. Wang, "Boundary-sensitive loss function with location constraint for hard region segmentation," *IEEE JBHI*, vol. 27, no. 2, pp. 992–1003, 2023.

[209] Y. Shi, H. Wang, H. Ji, H. Liu, Y. Li, N. He, D. Wei, Y. Huang, Q. Dai, J. Wu *et al.*, "A deep weakly semi-supervised framework for endoscopic lesion segmentation," *MedIA*, vol. 90, p. 102973, 2023.

[210] G.-P. Ji, D.-P. Fan, Y.-C. Chou, D. Dai, A. Liniger, and L. Van Gool, "Deep gradient learning for efficient camouflaged object detection," *MIR*, vol. 20, no. 1, pp. 92–108, 2023.

[211] T. Zhou, Y. Zhou, K. He, C. Gong, J. Yang, H. Fu, and D. Shen, "Cross-level feature aggregation network for polyp segmentation," *PR*, vol. 140, p. 109555, 2023.

[212] S. Jain, R. Atale, A. Gupta, U. Mishra, A. Seal, A. Ojha, J. Kuncewicz, and O. Krejcar, "Coinnet: A convolution-involution network with a novel statistical attention for automatic polyp segmentation," *IEEE TMI*, vol. 42, no. 12, pp. 3987–4000, 2023.

[213] N. K. Tomar, D. Jha, M. A. Riegler, H. D. Johansen, D. Johansen, J. Rittscher, P. Halvorsen, and S. Ali, "Fanet: A feedback attention network for improved biomedical image segmentation," *IEEE TNNLS*, vol. 34, no. 11, pp. 9375–9388, 2023.

[214] H. Shao, Q. Zeng, Q. Hou, and J. Yang, "Mcanet: Medical image segmentation with multi-scale cross-axis attention," *arXiv preprint arXiv:2312.08866*, 2023.

[215] H. Shao, Y. Zhang, and Q. Hou, "Polyper: Boundary sensitive polyp segmentation," in *AAAI*, 2024.

[216] M. M. Rahman, M. Munir, and R. Marculescu, "Emcad: Efficient multi-scale convolutional attention decoding for medical image segmentation," in *IEEE CVPR*, 2024.

[217] R. Schön, J. Lorenz, K. Ludwig, and R. Lienhart, "Adapting the segment anything model during usage in novel situations," in *IEEE CVPR*, 2024, pp. 3616–3626.

[218] L. Xie, M. Lin, T. Luan, C. Li, Y. Fang, Q. Shen, and Z. Wu, "Mhpflid: Model heterogeneous personalized federated learning via injection and distillation for medical data analysis," in *ICML*, 2024.

[219] H. Li, D. Zhang, J. Yao, L. Han, Z. Li, and J. Han, "Asps: Augmented segment anything model for polyp segmentation," in *MICCAI*, 2024.

[220] Z. Xu, F. Tang, Z. Chen, Z. Zhou, W. Wu, Y. Yang, Y. Liang, J. Jiang, X. Cai, and J. Su, " Polyp-Mamba: Polyp Segmentation with Visual Mamba ," in *MICCAI*, 2024.

[221] Y. Liu, Y. Tian, Y. Zhao, H. Yu, L. Xie, Y. Wang, Q. Ye, and Y. Liu, "Vmamba: Visual state space model," *NeurIPS*, 2024.

[222] J. Chai, Z. Luo, J. Gao, L. Dai, Y. Lai, and S. Li, " QueryNet: A Unified Framework for Accurate Polyp Segmentation and Detection ," in *MICCAI*, 2024.

[223] W. Wang, H. Sun, and X. Wang, " LSSNet: A Method for Colon Polyp Segmentation Based on Local Feature Supplementation and Shallow Feature Supplementation ," in *MICCAI*, 2024.

[224] X. Zhou and T. Chen, "Bsbp-rwkv: Background suppression with boundary preservation for efficient medical image segmentation," in *ACM MM*, 2024.

[225] B. Peng, E. Alcaide, Q. G. Anthony, A. Albalak, S. Arcadinho, S. Biderman, H. Cao, X. Cheng, M. N. Chung, L. Derczynski, X. Du, M. Grella, K. K. GV, X. He, H. Hou, P. Kazienko, J. Kocon, J. Kong, B. Koptyra, H. Lau, J. Lin, K. S. I. Mantri, F. Mom, A. Saito, G. Song, X. Tang, J. S. Wind, S. Woźniak, Z. Zhang, Q. Zhou, and R.-J. Zhu, "RWKV: Reinventing RNNs for the transformer era," in *EMNLP*, 2023.

[226] C. Wang, L. Wang, N. Wang, X. Wei, T. Feng, M. Wu, Q. Yao, and R. Zhang, "Cfatransunet: Channel-wise cross fusion attention and transformer for 2d medical image segmentation," *CIBM*, vol. 168, p. 107803, 2024.

[227] X. Jia, Y. Shen, J. Yang, R. Song, W. Zhang, M. Q.-H. Meng, J. C. Liao, and L. Xing, "Polypmixnet: Enhancing semi-supervised polyp segmentation with polyp-aware augmentation," *CIBM*, vol. 170, p. 108006, 2024.

[228] Z. Zhang, Y. Li, and B.-S. Shin, "Generalizable polyp segmentation via randomized global illumination augmentation," *IEEE JBHI*, vol. 28, no. 4, pp. 2138–2151, 2024.

[229] M. Wang, X. An, Z. Pei, N. Li, L. Zhang, G. Liu, and D. Ming, "An efficient multi-task synergetic network for polyp segmentation and classification," *IEEE JBHI*, vol. 28, no. 3, pp. 1228–1239, 2024.

[230] L. Yang, Y. Gu, G. Bian, and Y. Liu, "Msde-net: A multi-scale dual-encoding network for surgical instrument segmentation," *IEEE JBHI*, vol. 28, no. 7, pp. 4072–4083, 2024.

[231] G.-P. Ji, J. Zhang, D. Campbell, H. Xiong, and N. Barnes, "Rethinking polyp segmentation from an out-of-distribution perspective," *MIR*, vol. 21, no. 4, pp. 631–639, 2024.

[232] J. Ma, Y. He, F. Li, L. Han, C. You, and B. Wang, "Segment anything in medical images," *NComms*, vol. 15, no. 1, p. 654, 2024.

[233] Z. Liu, S. Zheng, X. Sun, Z. Zhu, Y. Zhao, X. Yang, and Y. Zhao, "The devil is in the boundary: Boundary-enhanced polyp segmentation," *IEEE TCSVT*, vol. 34, no. 7, pp. 5414–5423, 2024.

[234] Z. Lu, Y. Zhang, Y. Zhou, Y. Wu, and T. Zhou, "Domain-interactive contrastive learning and prototype-guided self-training for cross-domain polyp segmentation," *IEEE TMI*, 2024.

[235] J. Gao, Q. Lao, Q. Kang, P. Liu, C. Du, K. Li, and L. Zhang, "Boosting your context by dual similarity checkup for in-context learning medical image segmentation," *IEEE TMI*, 2024.

[236] C. Li, X. Liu, W. Li, C. Wang, H. Liu, and Y. Yuan, "U-kan makes strong backbone for medical image segmentation and generation," *arXiv preprint arXiv:2406.02918*, 2024.

[237] Z. Liu, Y. Wang, S. Vaidya, F. Ruehle, J. Halverson, M. Soljačić, T. Y. Hou, and M. Tegmark, "Kan: Kolmogorov-arnold networks," *arXiv preprint arXiv:2404.19756*, 2024.

[238] C. Fan, H. Yu, L. Wang, Y. Huang, L. Wang, and X. Jia, "Slice-mamba with neural architecture search for medical image segmentation," *arXiv preprint arXiv:2407.08481*, 2024.

[239] J. Xie, R. Liao, Z. Zhang, S. Yi, Y. Zhu, and G. Luo, "Promamba: Prompt-mamba for polyp segmentation," *arXiv preprint arXiv:2403.13660*, 2024.

[240] X. Xiong, Z. Wu, S. Tan, W. Li, F. Tang, Y. Chen, S. Li, J. Ma, and G. Li, "Sam2-unet: Segment anything 2 makes strong encoder for natural and medical image segmentation," *arXiv preprint arXiv:2408.08870*, 2024.

[241] J. G.-B. Puyal, K. K. Bhatia, P. Brandao, O. F. Ahmad, D. Toth, R. Kader, L. Lovat, P. Mountney, and D. Stoyanov, "Endoscopic polyp segmentation using a hybrid 2d/3d cnn," in *MICCAI*, 2020.

[242] G.-P. Ji, Y.-C. Chou, D.-P. Fan, G. Chen, H. Fu, D. Jha, and L. Shao, "Progressively normalized self-attention network for video polyp segmentation," in *MICCAI*, 2021.

[243] X. Zhao, Z. Wu, S. Tan, D.-J. Fan, Z. Li, X. Wan, and G. Li, "Semi-supervised spatial temporal attention network for video polyp segmentation," in *MICCAI*, 2022.

[244] X. Li, J. Xu, Y. Zhang, R. Feng, R.-W. Zhao, T. Zhang, X. Lu, and S. Gao, "Tccnet: Temporally consistent context-free network for semi-supervised video polyp segmentation." in *IJCAI*, 2022.

[245] J. G.-B. Puyal, P. Brandao, O. F. Ahmad, K. K. Bhatia, D. Toth, R. Kader, L. Lovat, P. Mountney, and D. Stoyanov, "Polyp detection on video colonoscopy using a hybrid 2d/3d cnn," *MedIA*, vol. 82, p. 102625, 2022.

[246] Z. Fang, X. Guo, J. Lin, H. Wu, and J. Qin, "An embedding-unleashing video polyp segmentation framework via region linking and scale alignment," in *AAAI*, 2024.

[247] H. Xu, Y. Yang, A. I. Aviles-Rivero, G. Yang, J. Qin, and L. Zhu, "Lgrnet: Local-global reciprocal network for uterine fibroid segmentation in ultrasound videos," in *MICCAI*, 2024.

[248] Q. Hu, Z. Yi, Y. Zhou, F. Peng, M. Liu, Q. Li, and Z. Wang, "Sali: Short-term alignment and long-term interaction network for colonoscopy video polyp segmentation," in *MICCAI*, 2024.

[249] Y. Lu, Y. Yang, Z. Xing, Q. Wang, and L. Zhu, "Diff-vps: Video polyp segmentation via a multi-task diffusion network with adversarial temporal reasoning," in *MICCAI*, 2024.

[250] L. Wan, C. Chen, Y. Xiao, J. Zhao, W. Feng, and H. Fu, "Iterative feedback-based models for image and video polyp segmentation," *CIBM*, vol. 177, p. 108569, 2024.

[251] Y.-C. Chou, B. Li, D.-P. Fan, A. Yuille, and Z. Zhou, "Acquiring weak annotations for tumor localization in temporal and volumetric data," *MIR*, vol. 21, no. 2, pp. 318–330, 2024.

[252] Z. Xu, J. Rittscher, and S. Ali, "Sstfb: Leveraging self-supervised pretext learning and temporal self-attention with feature branching for real-time video polyp segmentation," *arXiv preprint arXiv:2406.10200*, 2024.

[253] Y. Yang, Z. Xing, and L. Zhu, "Vivim: a video vision mamba for medical video object segmentation," *arXiv preprint arXiv:2401.14168*, 2024.

[254] G. Chen, J. Yang, X. Pu, G.-P. Ji, H. Xiong, Y. Pan, H. Cui, and Y. Xia, "Mast: Video polyp segmentation with a mixture-attention siamese transformer," *arXiv preprint arXiv:2401.12439*, 2024.

[255] B. Zhou, A. Khosla, A. Lapedriza, A. Oliva, and A. Torralba, "Learning deep features for discriminative localization," in *IEEE CVPR*, 2016.

[256] N. Carion, F. Massa, G. Synnaeve, N. Usunier, A. Kirillov, and S. Zagoruyko, "End-to-end object detection with transformers," in *ECCV*, 2020.

[257] S. Chen, P. Sun, Y. Song, and P. Luo, "Diffusiondet: Diffusion model for object detection," in *IEEE ICCV*, 2023.

[258] M.-M. Cheng and D.-P. Fan, "Structure-measure: A new way to evaluate foreground maps," *IJCV*, vol. 129, pp. 2622–2638, 2021.

[259] Z. Zhou, M. M. R. Siddiquee, N. Tajbakhsh, and J. Liang, "Unet++: Redesigning skip connections to exploit multiscale features in image segmentation," *IEEE TMI*, vol. 39, no. 6, pp. 1856–1867, 2019.

[260] O. Ronneberger, P. Fischer, and T. Brox, "U-net: Convolutional networks for biomedical image segmentation," in *MICCAI*, 2015.

[261] Q. Chen, X. Chen, H. Song, Z. Xiong, A. Yuille, C. Wei, and Z. Zhou, "Towards generalizable tumor synthesis," in *IEEE CVPR*, 2024.

[262] K. Tian, Y. Jiang, Z. Yuan, B. Peng, and L. Wang, "Visual autoregressive modeling: Scalable image generation via next-scale prediction," *arXiv preprint arXiv:2404.02905*, 2024.

[263] M. Hu, P. Xia, L. Wang, S. Yan, F. Tang, Z. Xu, Y. Luo, K. Song, J. Leitner, X. Cheng *et al.*, "Ophnet: A large-scale video benchmark for ophthalmic surgical workflow understanding," in *ECCV*, 2024.

[264] N. K. Tomar, D. Jha, U. Bagci, and S. Ali, "Tganet: Text-guided attention for improved polyp segmentation," in *MICCAI*, 2022.

[265] Y. Zhao, J. Li, L. Ren, and Z. Chen, "Dtan: Diffusion-based text attention network for medical image segmentation," *CIBM*, vol. 168, p. 107728, 2024.

[266] Y. Zhao, J. Li, and Z. Hua, "Tact: Text attention based cnn-transformer network for polyp segmentation," *IJIST*, vol. 34, 2023.

[267] Z. Qin, H. Yi, Q. Lao, and K. Li, "Medical image understanding with pretrained vision language models: A comprehensive study," in *ICLR*, 2023.

[268] M. Guo, H. Yi, Z. Qin, H. Wang, A. Men, and Q. Lao, "Multiple prompt fusion for zero-shot lesion detection using vision-language models," in *MICCAI*, 2023.

[269] L. H. Li, P. Zhang, H. Zhang, J. Yang, C. Li, Y. Zhong, L. Wang, L. Yuan, L. Zhang, J.-N. Hwang *et al.*, "Grounded language-image pre-training," in *IEEE CVPR*, 2022.

[270] S. Wang, Y. Zhu, X. Luo, Z. Yang, Y. Zhang, P. Fu, M. Wang, Z. Song, Q. Li, P. Zhou *et al.*, "Knowledge extraction and distillation from large-scale image-text colonoscopy records leveraging large language and vision models," *arXiv preprint arXiv:2310.11173*, 2023.

[271] R. Biswas, "Polyp-sam++: Can a text guided sam perform better for polyp segmentation?" *arXiv preprint arXiv:2308.06623*, 2023.

[272] Y. Zhao, Y. Zhou, Y. Zhang, Y. Wu, and T. Zhou, " TextPolyp: Point-supervised Polyp Segmentation with Text Cues ," in *MICCAI*, 2024.

[273] S. Wang, W. Zhou, Y. Yang, H. Huang, Z. Ye, T. Zhang, and D. Yang, "Adapting pre-trained visual and language models for medical image question answering," in *CLEF (Working notes)*, 2023.

[274] J. Li, D. Li, S. Savarese, and S. Hoi, "Blip-2: Bootstrapping language-image pre-training with frozen image encoders and large language models," in *ICML*, 2023.

[275] Z. Huang, F. Bianchi, M. Yuksekgonul, T. J. Montine, and J. Zou, "A visual–language foundation model for pathology image analysis using medical twitter," *NM*, vol. 29, no. 9, pp. 2307–2316, 2023.

[276] R. Taylor, M. Kardas, G. Cucurull, T. Scialom, A. Hartshorn, E. Saravia, A. Poulton, V. Kerkez, and R. Stojnic, "Galactica: A large language model for science," *arXiv preprint arXiv:2211.09085*, 2022.

[277] H. Liu, C. Li, Q. Wu, and Y. J. Lee, "Visual instruction tuning," in *NeurIPS*, 2024.

[278] C. Li, Y. Ge, D. Li, and Y. Shan, "Vision-language instruction tuning: A review and analysis," *TMLR*, 2024.

[279] G. Lupyan, R. A. Rahman, L. Boroditsky, and A. Clark, "Effects of language on visual perception," *TICS*, vol. 24, no. 11, pp. 930–944, 2020.

[280] C. Li, C. Wong, S. Zhang, N. Usuyama, H. Liu, J. Yang, T. Naumann, H. Poon, and J. Gao, "Llava-med: Training a large language-and-vision assistant for biomedicine in one day," in *NeurIPS*, 2024.

[281] M. A. Islam, S. Jia, and N. D. Bruce, "How much position information do convolutional neural networks encode?" in *ICLR*, 2020.

[282] E. J. Hu, P. Wallis, Z. Allen-Zhu, Y. Li, S. Wang, L. Wang, W. Chen *et al.*, "Lora: Low-rank adaptation of large language models," in *ICLR*, 2022.

[283] Y. Li, Y. Zhang, C. Wang, Z. Zhong, Y. Chen, R. Chu, S. Liu, and J. Jia, "Mini-gemini: Mining the potential of multi-modality vision language models," *arXiv preprint arXiv:2403.18814*, 2024.

[284] X. Chu, L. Qiao, X. Lin, S. Xu, Y. Yang, Y. Hu, F. Wei, X. Zhang, B. Zhang, X. Wei *et al.*, "Mobilevlm: A fast, reproducible and strong vision language assistant for mobile devices," *arXiv preprint arXiv:2312.16886*, 2023.

[285] S. Woo, S. Debnath, R. Hu, X. Chen, Z. Liu, I. S. Kweon, and S. Xie, "Convnext v2: Co-designing and scaling convnets with masked autoencoders," in *IEEE CVPR*, 2023.

[286] K. He, X. Chen, S. Xie, Y. Li, P. Dollár, and R. Girshick, "Masked autoencoders are scalable vision learners," in *IEEE CVPR*, 2023.

[287] M. Oquab, T. Darcet, T. Moutakanni, H. Vo, M. Szafraniec, V. Khalidov, P. Fernandez, D. Haziza, F. Massa, A. El-Nouby *et al.*, "Dinov2: Learning robust visual features without supervision," *TMLR*, 2024.

[288] A. Radford, J. W. Kim, C. Hallacy, A. Ramesh, G. Goh, S. Agarwal, G. Sastry, A. Askell, P. Mishkin, J. Clark *et al.*, "Learning transferable visual models from natural language supervision," in *ICML*, 2021.

[289] P. Villalobos, A. Ho, J. Sevilla, T. Besiroglu, L. Heim, and M. Hobbhahn, "Position: Will we run out of data? limits of llm scaling based on human-generated data," in *ICML*, 2024.

[290] B. Xiao, H. Wu, W. Xu, X. Dai, H. Hu, Y. Lu, M. Zeng, C. Liu, and L. Yuan, "Florence-2: Advancing a unified representation for a variety of vision tasks," in *IEEE CVPR*, 2024.

[291] D. Jiang, X. He, H. Zeng, C. Wei, M. Ku, Q. Liu, and W. Chen, "Mantis: Interleaved multi-image instruction tuning," *arXiv preprint arXiv:2405.01483*, 2024.

[292] J. B. Haurum, S. Escalera, G. W. Taylor, and T. B. Moeslund, "Which tokens to use? investigating token reduction in vision transformers," in *IEEE ICCV-W*, 2023.

[293] H. Diao, Y. Cui, X. Li, Y. Wang, H. Lu, and X. Wang, "Unveiling encoder-free vision-language models," in *NeurIPS*, 2024.

[294] Z. Chen, J. Wu, W. Wang, W. Su, G. Chen, S. Xing, M. Zhong, Q. Zhang, X. Zhu, L. Lu *et al.*, "Internvl: Scaling up vision foundation models and aligning for generic visual-linguistic tasks," in *IEEE CVPR*, 2024.

[295] G. Bachmann and V. Nagarajan, "The pitfalls of next-token prediction," in *ICML*, 2024.

[296] X. Huang, J. Wang, Y. Tang, Z. Zhang, H. Hu, J. Lu, L. Wang, and Z. Liu, "Segment and caption anything," in *IEEE CVPR*, 2024.

[297] Y. Kim, C. Park, H. Jeong, Y. S. Chan, X. Xu, D. McDuff, C. Breazeal, and H. W. Park, "Adaptive collaboration strategy for llms in medical decision making," in *NeurIPS*, 2024.